NANO · MICRO small
www.small-journal.com

Engineering Stress in Thin Films: An Innovative Pathway Toward 3D Micro and Nanosystems

*Thanh-An Truong, Tuan-Khoa Nguyen, Hangbo Zhao, Nhat-Khuong Nguyen, Toan Dinh, Yoonseok Park, Thanh Nguyen, Yusuke Yamauchi, Nam-Trung Nguyen, and Hoang-Phuong Phan**

Transformation of conventional 2D platforms into unusual 3D configurations provides exciting opportunities for sensors, electronics, optical devices, and biological systems. Engineering material properties or controlling and modulating stresses in thin films to pop-up 3D structures out of standard planar surfaces has been a highly active research topic over the last decade. Implementation of 3D micro and nanoarchitectures enables unprecedented functionalities including multiplexed, monolithic mechanical sensors, vertical integration of electronics components, and recording of neuron activities in 3D organoids. This paper provides an overview on stress engineering approaches to developing 3D functional microsystems. The paper systematically presents the origin of stresses generated in thin films and methods to transform a 2D design into an out-of-plane configuration. Different types of 3D micro and nanostructures, along with their applications in several areas are discussed. The paper concludes with current technical challenges and potential approaches and applications of this fast-growing research direction.

1. Introduction

Stress in thin films is a critical parameter for the performance of several complementary metal oxide semiconductors (CMOS) and micro/nanoelectromechanical systems (MEMS/NEMS) devices. In some cases, residual stress in thin films can cause problematic issues such as cracking,[1–5] peeling off,[6,7] buckling,[8–11] or blistering[12,13] that adversely influence the performance of electronics and sensing devices.[14] Understanding the nature of stress in thin film materials is critically important to ensure the functionality of CMOS and MEMS components. Engineering stresses in a well-controlled manner, on the other hand, is a powerful tool to enhance the performance of functional electronics devices. One of the first works that employed process-induced strain in modern transistors is the 90-nm generation logic technology for high-speed and low-power operation developed by Intel in the early of 2000, taking advantage of mobility enhancement in strained silicon.[15–17] Other well-known examples of strain engineering include the high electron mobility transistors (HEMT) employing the stress induced polarization, and mechanical sensors using of energy band deformation in stressed semiconductors.[18–22]

Recent years have witnessed a highly active research direction in the implementation of mechanical stresses to develop unconventional 3D micro/nanoarchitectures. These new 3D concepts introduce breakthrough functionalities that cannot be realized with standard 2D counterparts. For instances, for biological and tissue engineering applications, 3D structures better represent and mimic the complex shapes of biological constructs[23,24] thereby underpinning the fundamental investigation into intracellular and extracellular activities. 3D structures combined with biodegradable materials lay new concepts of bio-scaffolds for cell cultures and subsequent cell transplantation.[25–27] In photonics, 3D photonic crystals bypass the limitations in 2D structures, offering powerful tools for optical filters.[28] 3D architectures also offer a great potential for soft electronics with capability of forming conformal contact with biological tissues without fracturing under high strains.

T.-A. Truong, T.-K. Nguyen, N.-K. Nguyen, N.-T. Nguyen, H.-P. Phan
Queensland Micro and Nanotechnology Centre
Griffith University, Nathan
Queensland 4111, Australia
E-mail: h.phan@griffith.edu.au

H. Zhao
Department of Aerospace and Mechanical Engineering
University of Southern California
Los Angeles, CA 90089, USA

T. Dinh, T. Nguyen
Centre for Future Materials
University of Southern Queensland
Ipswich, Queensland 4305, Australia

Y. Park
Querrey Simpson Institute for Bioelectronics
Northwestern University
Evanston, IL 60208, USA

Y. Yamauchi
Australian Institute for Bioengineering and Nanotechnology
The University of Queensland
Brisbane, Queensland 4072, Australia

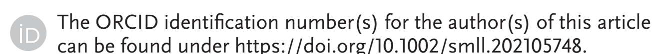
The ORCID identification number(s) for the author(s) of this article can be found under https://doi.org/10.1002/smll.202105748.

DOI: 10.1002/smll.202105748

 © 2021 Wiley-VCH GmbH

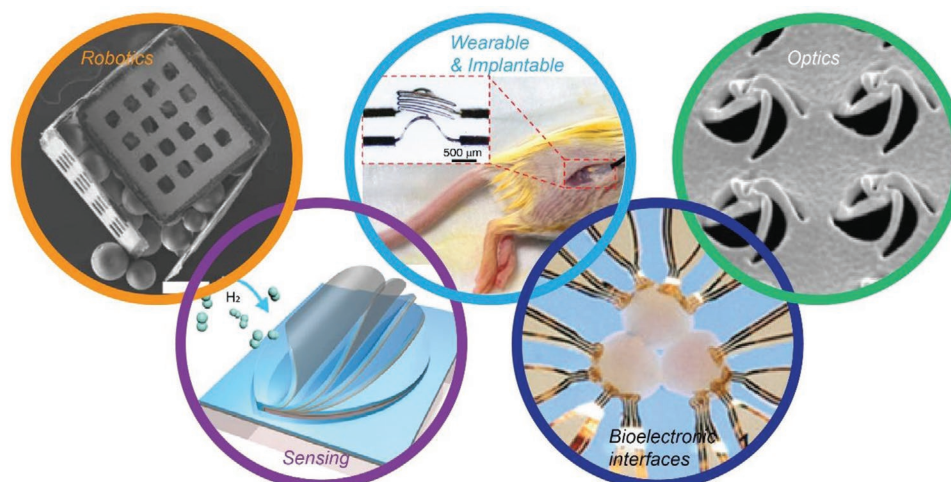

Figure 1. Five major applications of 3D structures fabricated base on stress-based approach: Robotics. Reproduced with permission.[62] Copyright 2014, Royal Society of Chemistry; wearable and implantable devices. Reproduced with permission.[63] Copyright 2019 Springer Nature; sensors. Reproduced with permission.[64] Copyright 2018, AAAS; tissue engineering and cell cultures, bioelectronics interfaces. Reproduced with permission.[65] Copyright 2021, AAAS; and optics. Reproduced with permission.[66] Copyright 2018, AAAS.

To realize 3D structures, several methods were proposed including bottom up,[29–33] and top down approaches.[34–49] The use of surface tension force is a common strategy to generate different designs such as actuators and micro-containers.[50–57] While this technique offers benefit of producing several 3D structures, it is challenging to achieve complex 3D geometries and to maintain 3D configurations. The other main drawback of this method is the requirement for complex fabrication steps and significant time consumption.[28] Process-induced stress approaches have been demonstrated to open new pathways to overcome those limitations. In this approach, stress or strain is deliberately introduced in thin films or substrates during the fabrication or growth process so that thin films can transform into 3D structures once the constraint between thin films and substrates is released. The stress can be generated by several ways such as lattice mismatch, deposition, thermal misfit, and substrate engineering. The versatility of this method allows for the use of a wide range of materials to build complex geometries, such as folded, bent, and twisted features.[28,58] These characteristics enabled the fabrication of new classes of functional devices ranging from sensors, optical devices, bioelectronic interfaces for tissue biological systems and to medical devices as shown in **Figure 1**.

Considering the emerging field of 3D microelectronics and MEMS in interdisciplinary applications, a review paper on this topic will bring significant benefits to the research communities and CMOS/MEMS designers. There are a number of review articles on the micro/nanofabrication of 3D structures.[25,28,58–61] However, a comprehensive view of the stress-based technologies, from physical aspects to engineering approaches, is missed from these works. For instance, previous reports focused on several fabrication approaches and lacked an elaborate view on the principle and utilization of stress in thin films. Therefore, this paper aims to provide a systematic overview of the state-of-the-art approaches using engineering strains in thin films for constructing variable micro/nanoarchitectures and their potential applications. The paper starts with the physical background of stress generation mechanisms in different types of materials. Next, different fabrication routes to form several 3D architectures tailoring unique engineering stress approaches are highlighted. Applications of these 3D structures in interdisciplinary areas such as robotics, bio-electronic interfaces, optical systems, and physical/chemical sensing are discussed. Finally, the paper concludes with the current status and outlines a perspective on future research directions of strain engineering.

2. Principle of Stress in Thin Film

Residual stresses occur due to misfitting in natural shape between different regions, parts, or phases.[67] Stresses in thin film are attributed to different factors and can be categorized based on physical phenomena, properties, and applications. For example, Hu and Huang[68] classified stress in thin films into three categories based on their origins, which are thermal stress from the differences in coefficients of thermal expansion (CTE), interfacial stress due to differences in lattice structure, and intrinsic stress caused by the deposition processes. From the fabrication approach point of view, we classify stresses into four group of i) intrinsic (growth) stress, ii) epitaxy stress (lattice mismatch stress), iii) stress generated from micro/nanomachining, and iv) stress in active materials under external stimuli.

2.1. Intrinsic Stress

To date, the origin of stress in grown films is still a challenging research question, driving extensive theoretical and experimental investigations.[69] Several models have been developed to comprehensively explain the physical phenomena causing the formation of stresses.[68–74]

Atomic rearrangement is a main cause of mechanical stress in epitaxial films, where chemical bonding between a film and

 © 2021 Wiley-VCH GmbH

its seeding substrate generates an intrinsic stress.[69,72] This stress can originate from several factors such as non-equilibrium growth,[69,75–77] grain growth[73,78] excess vacancy annihilation,[69] grain boundary relaxation,[79] shrinkage of grain boundary voids,[74] and impurities.[80,81] In addition, phase transformation and precipitation,[82–84] lattice mismatch, the surface energy/tension,[85–87] and absorption[88] are critical phenomena contributing to the atomic rearrangement and the resultant residual stress. Surface tension typically causes compressive stress while the other factors are likely to create compressive stress at the initial growth stage and then transferring to tensile stress when the film is eventually deposited.[72,89] It noteworthy that stress generated by sputtering or high energetic deposition is likely to be compressive.[72]

Thornton's model[73] described microstructure change under varying deposition temperature relative to the melting point of materials. As illustrated in **Figure 2**a, the sizes and shapes of grains can vary due to atomic mobility, which can be driven by deposition temperature or material characteristics. Materials with low atomic mobility are distinguished by zone I. These have columnar

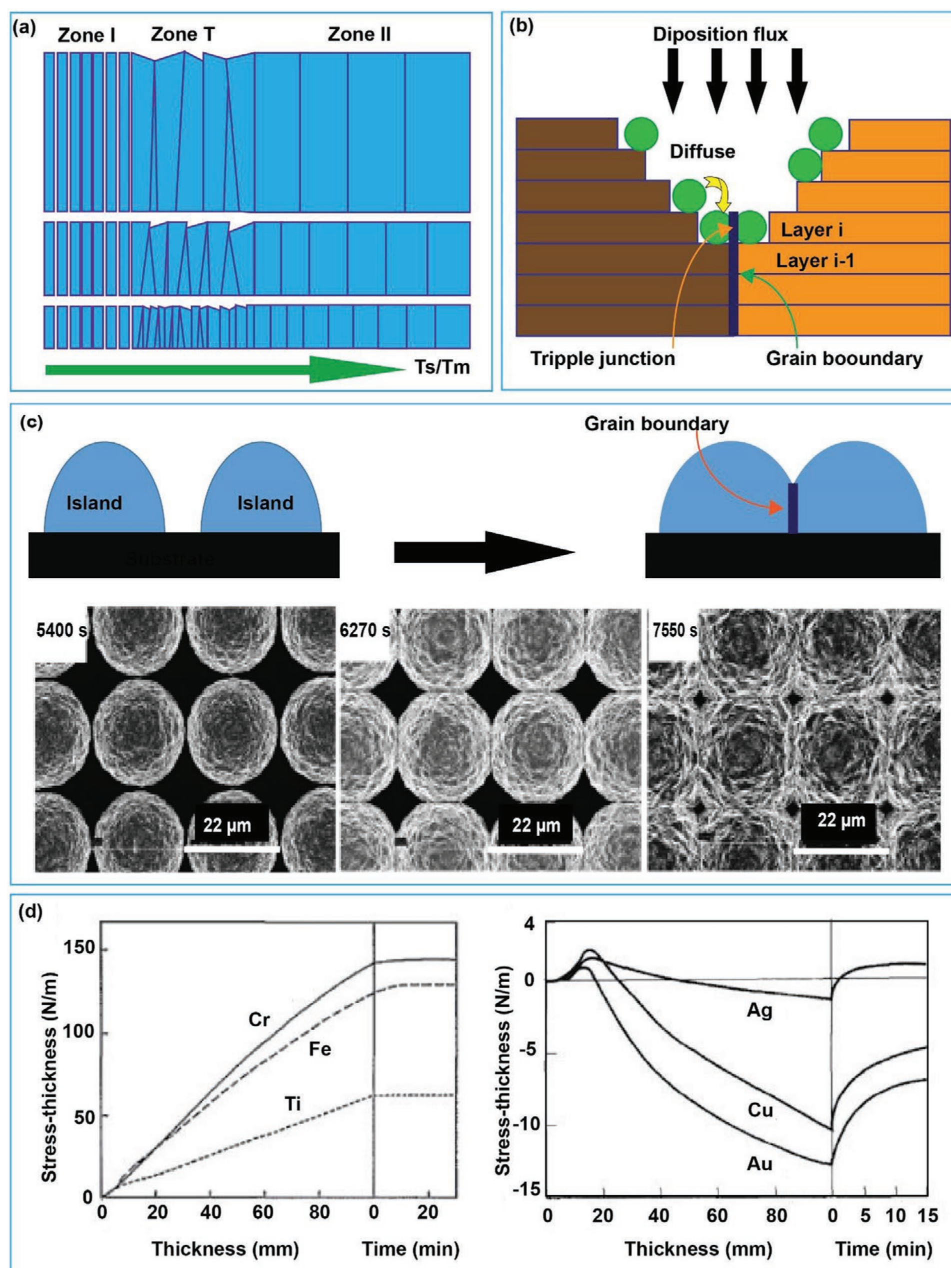

Figure 2. Intrinsic stress generation models. a) Model to describe the evolution of grain size with thickness at different deposition temperature, where T_s is the deposition temperature and T_m is the melting point.[73] b) Kinetic model to describe stress at triple junction during film growth.[90] c) Tensile stress generated due to coalescence of Ni islands. Reproduced with permission.[92] Copyright 2014, AIP Publishing. d) Stress-thickness evolution during vapor-phase growth in low mobility (type I, left) and high mobility (type II, right) materials. Reproduced with permission.[95] Copyright 1990, Elsevier.

© 2021 Wiley-VCH GmbH

and uniform shapes and sizes along thickness direction, and thereby stress does not vary with thickness. The transition zone, namely T, is for materials with slightly higher atomic mobility. Their grain sizes grow larger at the top than at the bottom, which can modify stress of the next deposited layer. For high atomic mobility materials in zone II, the grain size is significantly larger and varies along the thickness of the film. As atomic density at the grain boundary is lower than that in their bulk forms, the densification of grain boundaries when reducing temperature leads to a shrinkage of the film volume. This volume change results in a residual stress if the film is constrained to a substrate.

Another comprehensive kinetic model was proposed to incorporate more parameters such as material, deposition rate, grain size and diffusivity,[78,90] Figure 2b. Accordingly, high diffusivity atoms can bond together at triple junction of adjacent islands and form a new segment of grain boundary that can modify the stress of the existing layer. The development of tensile stress in thin film is often explained by the grain boundary formation during the coalescence of islands. During coalescence, two or more atomics islands merge into a single cluster.[91] Figure 2c shows a schematic model and SEM images of Ni islands that well represents this phenomenon.[92]

The above three models lay the foundation for the current theoretical studies of mechanisms of stress formation in thin film,[78,79,90,92–94] where material properties, deposition temperature and growth rate are typically taken into account. In terms of material characteristics, melting point and atomic mobility play an important role.[69,72,95] Abermann[95] classified materials into two types. Type I is materials with low atomic mobility and high melting temperature such as Mo, Ta, and W. Their stress is likely to be tensile regardless of the grown film thickness, Figure 2d (left). Type II includes materials having high atomic mobility and low melting temperature (e.g., Ag), Figure 2d (right). Stress tends to transition from tensile to compressive as grown films become thicker and relax. On the other hand, temperature is a key factor affecting the change of stress behaviors in thin film.[69,72,89] At a high temperature, type I materials exhibit the same behavior as type II as high temperature can increase the mobility of atoms. In addition, growth rates also modify stress in thin film significantly. Higher growth rates result in more compressive stress during sputtering while lower growth rates lead to more tensile stress in low energetic deposition processes.[72,89]

2.2. Stress Caused by the Lattice Mismatch in Epitaxial Films

The differences between lattice structures of thin films and the underlying layers result in considerable stress gradients. **Figure 3**a illustrates the principle of stress due to lattice mismatch. The layer with a smaller lattice constant experiences a tensile stress and the layer with greater lattice constant shows a compressive stress. The lattice mismatch strain is calculated as:

$$\varepsilon_{mf} = \frac{a_s - a_f}{a_s} \tag{1}$$

where ε_{mf} is misfit strain, a_s and a_f are lattice constants of the substrate and film, respectively. As epitaxy stress and thermal stress originated from the same source, which is the misfit in properties of different materials, they are often realized to co-exist. Suhir et al. proposed a mathematical model to assess stress in a GaN film deposited on a SiC substrate.[96] Accordingly, stress generated from only a 3% lattice mismatch is significantly higher than that due to temperature variation, even at a high growth temperature of 1000 °C. For some material systems such as silicon-on-sapphire, stresses resulted from lattice mismatch and thermal expansion typically do not exhibit thickness-dependence phenomenon when the thickness ratio between the substrate (sapphire) and the thin film (silicon) reached over 20.[97] In practical silicon-on-sapphire based devices, this thickness ratio is designed at around 100 to obtain a uniform and controllable normal residual stress. Furthermore, dislocations often occur at the interface of two epitaxial layers, causing a variation in the stress profile of thin films. Therefore, disclocation, CTE mismatch, and lattice mismatch must be taken into account for analytical models of stress in bilayers thin films.

2.3. Thermal Stress

Thermal stress typically arises from the differences in the coefficient of thermal expansion (CTE) of stacking layers, which can be defined as: $\Delta \sigma_{thermal} = M_f(\alpha_s - \alpha_f)\Delta T$, where M_f is the biaxial modulus of the thin film, while α_s and α_f are CTE of the substrate and film, respectively. Thermal stress has a detrimental effect on 2D electronics devices such as the generation of buckling in 2D devices.[100] However, this stress is a useful tool to produce 3D structures as stress can be generated in a bilayer of two different materials when temperature changes. The thermal stress leads to the formation of 3D structures if the bilayer thin film is released from the attached under layers or substrates. Although the concept of thermal stress is relatively simple, a comprehensive study on thermal mismatch stress between multiple layers is imperative to tailor this type of stress for the development of complex 3D configurations. For instance, employing analytical and simulation, Haider et al. demonstrated linear relationships between thermal stress versus the growth temperature, the Young's modulus of thin films, and thickness of substrates in TiN physically deposited on stainless steel, as shown in Figure 3c.[98] Another study reported by Yang et al. employing finite element analysis showed a relatively similar trend in a Ni thin film on a H62 Cu plate, where the thermal stress increases as temperature increases.[99] However, stress distribution in this thin film is not uniform due to the nonuniform thickness of thin film and substrate.

2.4. Stress Induced from Micro/Nanofabrication Processes

Several fabrication methods exist for micro- and nano-scale features. These methods are likely to produce stress in thin films and substrates. While stresses can be unwanted in the case of wafer bonding,[101,102,111,103–110] surface passivation,[112–116] laser shock peening,[117,118,127,119–126] and laser machining[128,129] they are deliberately introduced in thin films and/ or substrates to

© 2021 Wiley-VCH GmbH

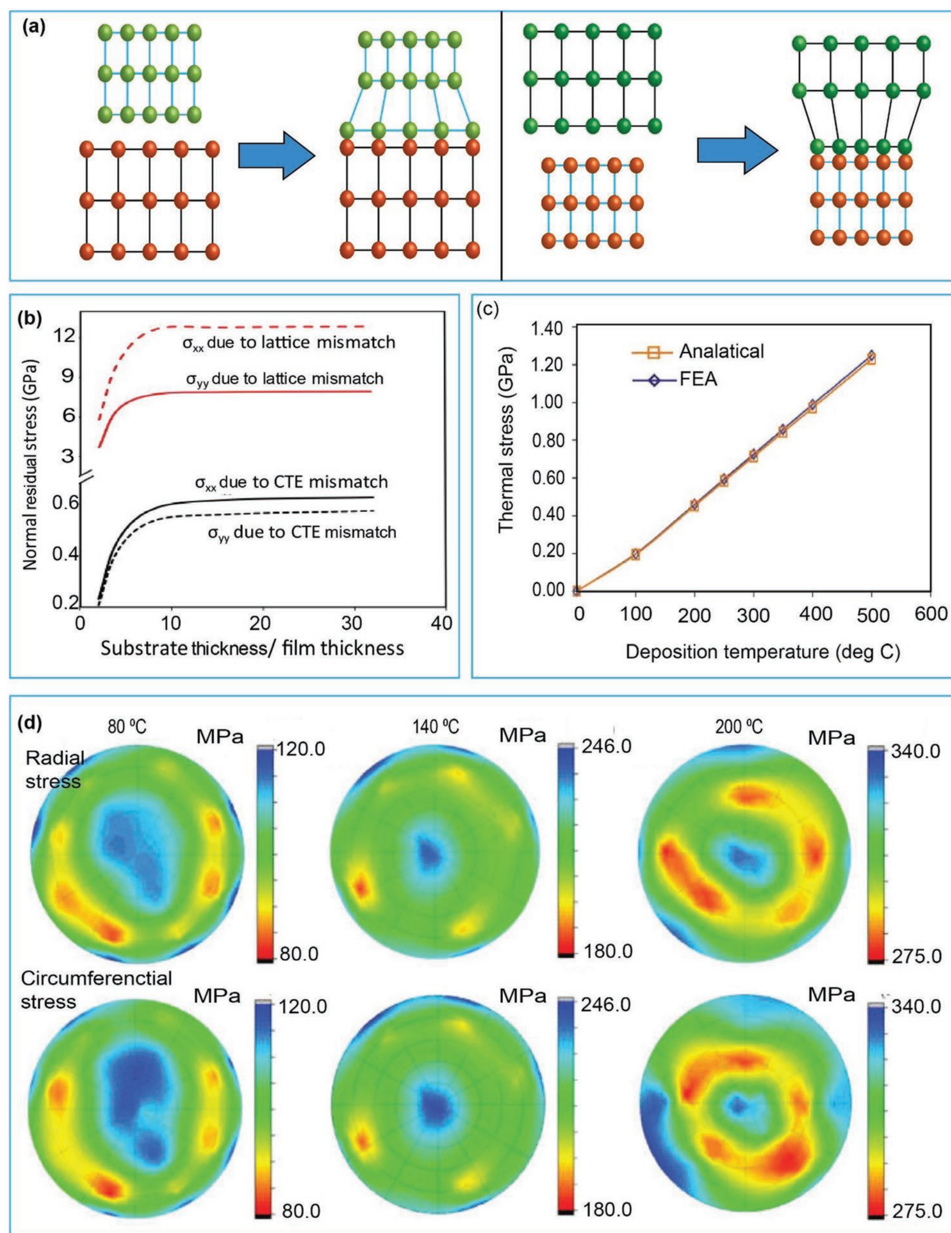

Figure 3. a) Mechanism of lattice mismatch stress. b) Variation of residual stress caused by lattice mismatch and thermal mismatch versus film thickness of silicon on sapphire films. Reproduced with permission.[97] Copyright 2013, Elsevier. c) Relationship of thermal stress and deposition rate of TiN thin films on stainless steel substrates. Reproduced with permission.[98] Copyright 2005, Elsevier. d) Finite element analysis result of thermal stress distribution in Ni thin film electroplated on H62Cu plate at different temperatures Reproduced with permission[99] Copyright 2021, Copyright MDPI.

form 3D structures in other fabrication methods. This section only reviews methods which have been used stress as a tool to produce 3D structures.

2.4.1. Ion Implantation

Ion implantation is widely employed for micro/nanomachining,[130–132] surface modification and imaging,[133] as well as impurity doping.[134–136] This technique is also applied to induce or engineer stress in thin films,[137–139] where ion species, dose energy and density can be well controlled to achieve the desired 3D structures. As such, higher implanting energy and dose density can reduce greater residual stress as ions can penetrate deeper and collide with lattice atoms. Sufficient implantation energy and dose density combined with annealing can result in fewer defects of thin films. Ions of atoms with greater atomic radius can generate larger stress.[140] Stress induced by ion implantation is either compressive or tensile, offering versatile routes to create complex 3D shapes via controlling bending angles and bending direction (upward or downward). **Figure 4**a illustrates the mechanism of residual stress,[66,141,142] where ions

© 2021 Wiley-VCH GmbH

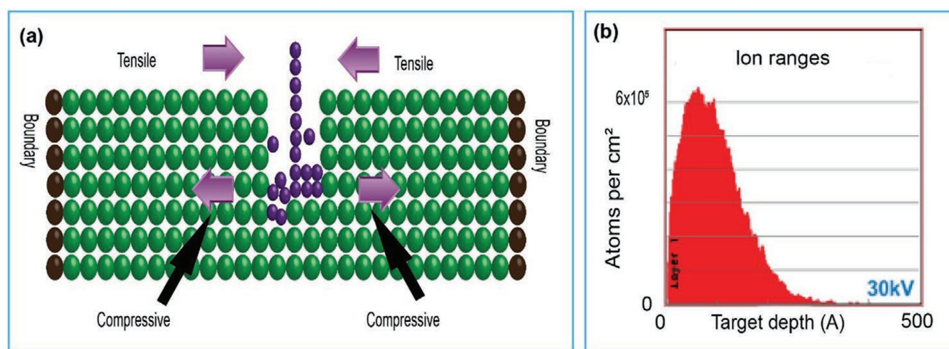

Figure 4. a) Schematic illustration of stress generated by FIB mechanism. b) SRIM plot of gallium ion concentration and vacancy density as a function of Au film depth under ion beam acceleration voltage of 30 kV. Reproduced with permission.[66] Copyright 2018, AAAS.

are implanted into lattice structure, whilst atoms at the surface of the film are bombarded. Subsequently, the bulk structure of the film is damaged, and irradiated ions form a new layer. As a result, surface vacancies lead to coalescence of the grain, which causes tensile stress near the film surface. Ions inserted into the bulk structure increase bulk volume and causes a compressive stress. Figure 4b shows the SRIM simulation of focus ion beam (FIB) implantation of Gallium ion onto an Au thin film. Ions are inserted into the films within a depth up to 50 nm. Experiment showed that 30 kV Ga ion beam irradiated onto 80-nm thick Au film results in tensile stress.[66] To induce a compressive stress, gaseous ions with high enough energy should be used to implant ions into a depth of one quarter the membrane thickness.[143] Tensile stress also occurs when light ion such as H^+ or He^+ is implanted into vitreous silica.[144]

2.4.2. Stress Due to Substrate Deformations

The substrate deformation approach uses pre-strained elastomer substrates to produce 3D structures from 2D layouts. The assembly consists of three main steps as shown in **Figure 5**a.[58] Initially, planar structures (referred to as "2D precursors") are patterned on a rigid substrate, followed by the deposition of bonding sites. The next step involves the transfer of 2D precursors onto a pre-stretched elastomer, and bonding of the 2D precursors to the substrate at desired locations. Finally, release of the pre-strained elastomer produces compressive stresses to the 2D precursors via the bonding sites, causing unbonded regions to buckle out of plane to form 3D buckling structures. Elastomer substrates can be stretched and released using thermal[145] or mechanical methods.

Several theoretical frameworks and analytical studies were reported to elucidate the relationship between buckling profile and the pre-straining approach.[145–152] Typically, buckling only occurs when the pre-strain reaches the critical threshold. Jiang et al. [145] showed that buckling amplitude and wavelength increase with the width of microribbons bonded on to a soft substrate. The maximum strain in buckling structure is much smaller than the pre-strain induced in the substrate, offering stretchability to 3D microstructures.[153–155]

Engineered stress and strain in 2D thin films combined with pre-strain substrate enable the development of interesting 3D structures. For instance, nonuniform 3D shapes can be produced on monolayer of a material which has partially varied thickness. This nonuniform thickness leads to different pattern of strain on the film with smaller strain at thicker parts. Relaxing pre-strained substrate results in partially varying degree of compressive buckling on precursor, Figure 5b.[156] In another example, inserting a tensile or compressive pre-stressed Au beam onto 2D precursors could control 3D shape to pop down or pop up, Figure 5c.[157] Varying pre-strain and modifying the substrate increase the degree-of-freedom in 3D architectures. Furthermore, complex 3D shapes can also be formed by controlling the sequences and directions of releasing pre-strain,[158,159] where releasing stress following different paths leads to distinct configurations even from the same specialized 2D precursor, Figure 5d.[159] Modification of the hosting substrate offers additional routes to engineer 3D micro configurations as demonstrated in a paper reported by Zhao et al. using PDMS with cut-out features.[158] Specifically, in this work, the authors induced a biaxial pre-strain up to 100% to the patterned PDMS substrate that causes adjacent units of PDMS to rotate in opposite directions. The rotation angle reached its maximum at a strain of ≈40%. Therefore, releasing the biaxial strain of the substrates from 100% down to 40% creates a compressive stress, leading to structural buckling. Further relaxing PDMS to the stress-free state (i.e., 0%) triggers a shear stress at each unit, resulting in a twisting transformation, Figure 5e.

A combination of the buckling method and Kirigami technique can enhance mechanical stretchability and the robustness of 3D structures. Figure 5f demonstrates some examples of this hybrid technique, where the maximum strain in 3D Kirigami structures was much smaller than that of 3D Origami shapes without cutting of precursors.[160] In contrast, Kirigami with cut features have been demonstrated as a versatile technique for a broad range of 3D geometries due to a lower stress concentration.[160]

2.4.3. Stress Induced in stimuli-responsive materials

Stress gradients are induced by the response of material under external stimuli such as heat,[161,162] light,[163,164] electron beam,[165,166] and pH.[167] These interesting properties open a new way for a self-assembly of 3D structures from 2D thin films.

 © 2021 Wiley-VCH GmbH

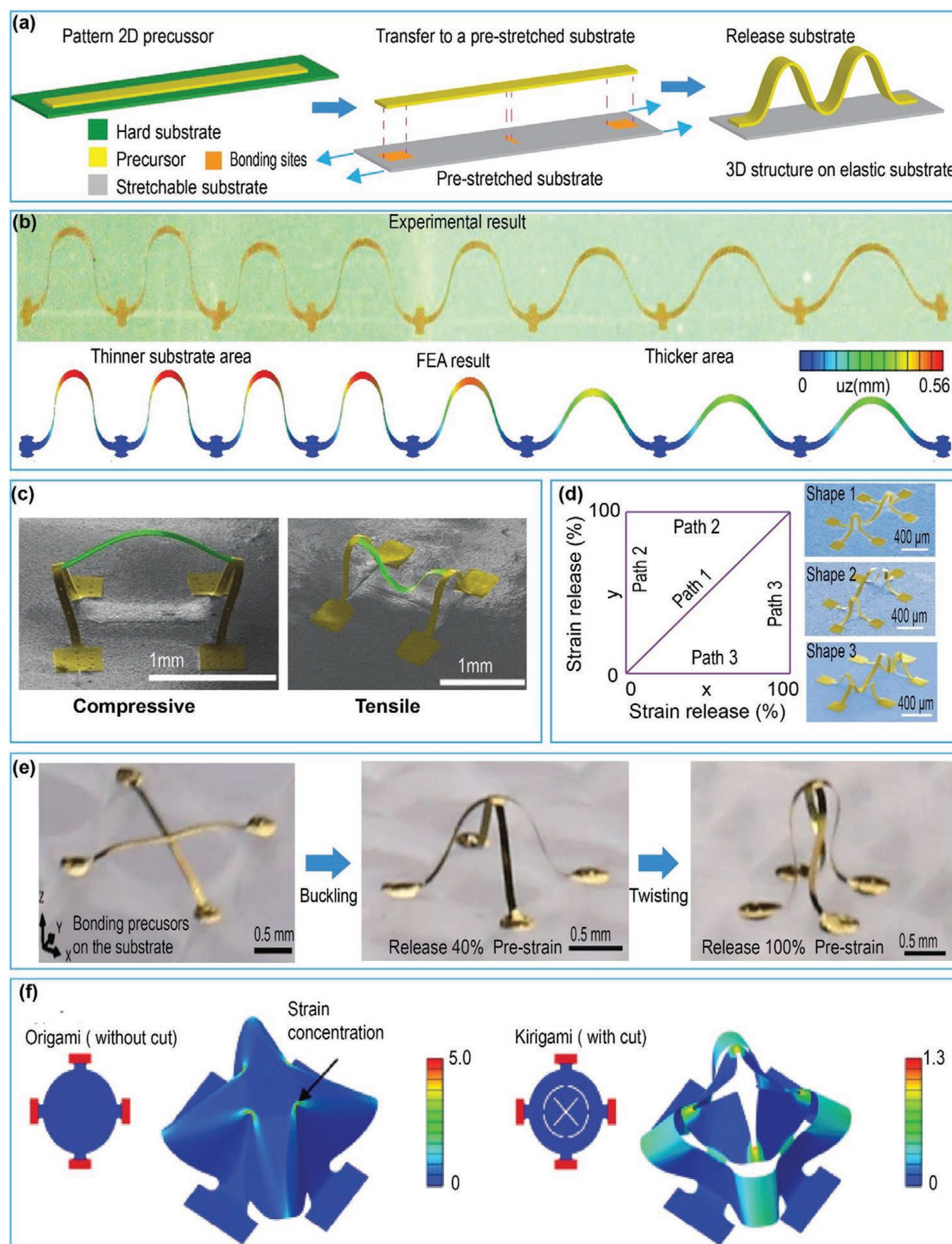

Figure 5. Stress due to substrate engineering approach: a) Schematic illustration of the assembly of 3D structures base on substrate deformation approach. b) Nonuniform 3D structures on a single substrate with varying thicknesses. Reproduced with permission.[156] Copyright 2016, John Wiley and Sons; c) Engineering pre-stress on 2D precursors to generate different bending structures. Reproduced with permission.[157] Copyright 2017, John Wiley and Sons; d) releasing of pre-strained substrates in three different paths results in three distinct 3D shapes. Reproduced with permission.[159] Copyright 2018, Springer Nature; e) twisting and buckling transformation of a substrate and precursor on it generated by different releasing amount of pre-strain. Reproduced with permission.[158] Copyright 2019, National Academy of Sciences; f) comparison of strain concentration between Origami and Kirigami precursors. Reproduced with permission.[160] Copyright 2015, PNAS.

The most common materials for this approach are cross-linkable polymers. Low exposure of SU-8 films to ultraviolet lights creates cross link gradients.[168] Removing non-cross-linked material by de-solvation triggers a larger volume change in the less cross-linked portion. This difference in the volume change creates a stress gradient along the film thickness, causing a bending of the film toward the less cross-linked side. On the other hand, solvation (i.e., immersing a film into a solution with similar solubility parameters such as acetone), makes the less cross-linked network to absorb the solution and relieve the stress gradient, leading to the folding and unfolding of 2D thin films.[169] Furthermore, temperature can change the cross link density of shape-memory polymers. Thus, changing temperature around crystallizing temperature and melting temperature can lead to a stress formation and stress release process.[170]

© 2021 Wiley-VCH GmbH

Another example of stimuli-responsive materials is polymethyl methacrylate (PMMA) under electron beam irradiation.[165] Applying a low energy e-beam can break the bonds of polymer chains inside PMMA, namely chain scissions. Chain scissions lead to outgassing, which creates and emits decomposition gasses from the PMMA. These phenomena result in a volume shrinkage in the PMMA film. This shrinkage is distributed partially inside a homogeneous PMMA film under a proper e-beam parameter and generates a stress gradient. The stress profile can be tuned by changing the irradiating locations as shown in, or by focusing the maximum e-beam energy at targeted positions along the depth of PMMA.

2.5. Measurement of Stress in Thin Film

Understanding the stress in thin film is of critical importance for the subsequent engineering approaches for 3D architectures. Measuring techniques can be classified into destructive and nondestructive methods. Destructive methods are often straightforward and accurate. They, however, cause fracture on the surface of testing samples that is sometimes unacceptable. Nondestructive methods are non-contact and can offer high resolution. These methods, however, often requires expensive equipment. The most ubiquitous methods to quantify stress are measurement of curvature,[171,172] X-Ray diffraction,[173–179] Raman spectroscopy,[180–182] and FIB analysis.[183–185]

2.5.1. Measurement of Curvature

This technique measures the curvature of the substrate using non-contact methods (e.g., profilometry, strain gauges) or contact methods (e.g., laser scanning, grid, white light interferometer, and double crystal diffraction topology).[186,187] The Stoney Equation (2) describes the relationship between the measured curvature and the average stress:[188,189]

$$\kappa = \frac{6\bar{\sigma}h_f}{M_s h_s^2} \tag{2}$$

where M_s and h_s are the biaxial modulus and thickness of the substrate respectively; and κ, $\bar{\sigma}$, h_f are the curvature, average stress and thickness of the measured film, respectively. The Stoney equation can only be applied under several assumptions such as a uniform thickness in both films and substrates with homogeneous, isotropic, and linearly elastic properties, along with the infinitesimal strains and rotations of the plate system.[190] Therefore, while this is a simple method, it is not suitable for measuring complex strain in anisotropic materials. Some modifications for the Stoney equation were proposed to improve the accuracy of stress estimation.[190–193]

2.5.2. X-Ray Diffraction Method

When a crystalline material is subjected to a mechanical stress, its atomic spacing changes and can be detected using X-ray diffraction (XRD) following the Bragg's law. This method requires an assumption of a plane-stress state in thin films.[179] An X-ray beam is projected at the incident angle of Ω to a sample surface which has an off axis angle ψ with respect to its normal plane. The crystalline grain lying on the (*hkl*) lattice plane emits an XRD beam at a diffraction angle of 2θ. The strain (ε) is then given by Equation (3).

$$\varepsilon = \left(\frac{1+\nu}{E}\right)\cdot\sigma_{\Phi\Phi}\cdot\sin^2(\psi) - \frac{\nu}{E}(\sigma_1+\sigma_2) \tag{3}$$

where E and ν are Young modulus and Poission ratio of the measured material in the direction normal to the (*hkl*) plane respectively; and σ_1 and σ_2 are two in-plane stresses. It is often assumed that $\sigma_1 = \sigma_2 = \sigma$ and the above equation can be further simplified. The Bragg diffraction angle 2θ can be measured at each diffraction peak, and the tilt angle ψ is calculated as $\psi = \theta - \Omega$. The accuracy of this method depends on several factors such as tested material, instrument set up and data processing.[179]

2.5.3. Raman Spectroscopy

Mechanical stress or strain can modify the frequency of the Raman mode. Quantify the shift of the peak position of the Raman spectrum in a strained thin film compare to that of a stress-free thin film can determine the sign and magnitude of residual stress.[177] For instance, compressive stress will increase Raman frequency, while tensile stress will result in a decrease.[194] Equation 4 describes the relation between peak shift and the stress.[195]

$$\Delta\omega = \omega_\sigma - \omega_f = S \times \Delta\sigma \tag{4}$$

where $\Delta\omega$ is the peak shift, ω_σ and ω_f are the peak positions at the stressed condition, and the stress-free condition, respectively, S is the stress-related coefficient, and $\Delta\sigma$ is the measured stress. Raman spectroscopy method is non-contact, high-resolution, and applicable for amorphous materials. One challenge of this method is that the effect of temperature on the phonon frequency often dominates that of thermal stress.[196]

2.5.4. FIB Analysis

One the most popular destructive methods to measure stress in thin film is FIB-base analysis. This technique combines FIB milling, scanning electron microscopy (SEM) and digital image correlation (DIC) to provide ultra-high resolutions for the residual stress analysis. In particular, FIB is used as an incremental milling tool to mill selected geometry. SEM captures images before and after milling. Finally, comparing measured strain with the result from finite element analysis provides the through-thickness profile of residual stress. This method is applicable for a wide range of materials including amorphous materials.

3. 3D Architectures Using Stress in Thin Films

Stress-induced approaches enable fabrication of several 3D structures with various feature size ranging from nanometers

 © 2021 Wiley-VCH GmbH

(e.g., using epitaxial stresses) up to several centimeters (e.g., using substrate deformation approach). This broad range of dimensions in 3D architectures lays a versatile platform for both micro- (i.e., photon–plasmon coupling) and macro-scale (e.g., wearable electronics) applications.

3.1. Out-of-Plane Bending Cantilevers

Residual stress offers attractive features to form out-of-plane structures. For instance, a monolayer with a stress gradient along its thickness can lead to an out-of-plane bending. However, controlling stress in a monolayer film depends on several parameters, and is relatively challenging.[200] Another approach is the use of multiple layers with a variation of thermal stress[197,198,201,202] or epitaxial stress.[203–206] The bending angles and directions can be engineered by inducing a tensile or compressive stress in each layer from the growth process[200,207] The residual stress technique has been applied in various materials such as SiC,[199] SiN,[208–210] SiO_x,[198,202] and AlN.[197,211]

Figure 6a shows a typical procedure for fabrication of a standing piezoresistive cantilever,[197] which can be generalized for all types of out-of-plane structures. First, pre-strained material layers are deposited onto a sacrificial layer. The piezoresistors and contact pads are then deposited onto that strained layer for the case of piezoresistive sensors. After patterning the 2D films to for the desired structures, the out-of-plane shapes can be achieved by etching the sacrificial layers. Figure 6b shows SEM images of AlN/Mo cantilever popped out of the Si substrate.[197] The bending level of these cantilevers depends on the residual stress of pre-strained AlN/Mo layers, which can be controlled by deposition parameters and cantilever geometry (e.g., length and thickness). Figure 6c shows example of curved-up microcantilevers of two layers of SiO_2.[198] The Si piezoresistive layer is sandwiched between the SiO_2 layers so that it can be protected from fluids or particles in working environments. However, the sensitivity of the sensor made from this structure is proportional to the distance from the neutral plane of the cantilever to the piezoresistor. This means that the SiO_2 cap layer should be as thin as possible and the lower SiO_2 layer should be thicker, increasing the stiffness of the beam and the protection effect of the cap layer. Therefore, the design should optimize the thickness of two SiO_2 layers. The study from cantilevers of SiC showed that the bending direction of the beams depend on their thickness, Figure 6d. Furthermore, the bending level of these beams depend on their length.

3.2. Micro/Nanotubes and Helices

Micro/nanotubes offer interesting features such as large surface areas for chemical sensing, and hollow structures for effective drug delivery.[212] A similar fabrication pathway as that of the above out-of-plane structures can be applied to form micro/nanotubes. The main difference between these two groups of configurations is the large deflection in micro/nanotubes that allows released cantilevers to roll up and form enclosed circular shapes. A typical fabrication process of micro/nanotubes starts with the deposition of a sacrificial layer onto a substrate. Subsequently, pre-stressed functional layers are deposited onto this sacrificial film. The sacrificial layer is removed, allowing the functional layers to roll into a tube. The rolling direction generally follows the stress gradient,[58] enabling the formation of micro/nanotubes with both clockwise and anticlockwise rolling directions.[213] This simple but high throughput approach has been demonstrated in a broad range of materials.[213–221]

The formation of micro/nanotube depends on the magnitude and gradient of stress developed in functional layers. The two main methods to generate stress in functional layers are the intrinsic stress due to non-epitaxial growth, and epitaxial stress resulted from hetero-deposition.[222] **Figure 7**a presents the concept of the former approach, where the residual stress depends on the CTE mismatch between the sacrificial layers and deposited films, the deposition rate, and stress evolution.[218] Additionally, removal of the sacrificial layer is a critical step, where etching-selectivity between the sacrificial layer and the functional layer should be over 1000:1.[223] Furthermore, a study on TiO_2 showed that a longer etching time leads to more cylindrical tubes.[215] The non-epitaxial growth is further enhanced using a dry fluorocarbon-assisted rolling approach, where the etching step for sacrificial layers is eliminated. The CTE mismatch between the strained layer, the fluorocarbon film and the substrate cause the functional layer to detach and roll up, Figure 7b.[224] A week bonding between the strained layer and the fluorocarbon film is the key to facilitate this detachment. This approach is advantageous for creating highly symmetric and multi-winding micro tubes.[224]

The later method employs an heteroepitaxial growth of multiple layers with different lattice constants, Figure 7c.[225] The demerit of this technique is the amorphous or polycrystalline morphology in the as-grown films, which are relatively unstable and thus requiring critical point drying to prevent tubes from collapsing.[223] However, the heteroepitaxial approach possess several advantages such as tunability of bending angles based on the lattice mismatch,[223] and controlling of the rolling direction (i.e., up or down) by switching the relative position of the deposited layers.[58,59,226,227] For instance, the diameter of the heteroepitaxial tube (D) can be tuned by changing the thickness of functional layers (d) and strain level (ε).[218] For a tube with symmetric bilayers (with thicknesses of d_1 and d_2), its rolling diameter is given by: $D = (d_1 + d_2)^3 / (3\varepsilon d_1 d_2)$.[206,217,227–229] In the heteroepitaxial approach, one of the as-deposited film can be treated as a sacrificial layer to further facilitate the detachment and rolling.

Rolling of 2D cantilevers with a twisted angle and numerous turns can form helical microarchitectures.[230–232] For instance, the orientation and pitch of InGaAs/GaAs helices depends on the angle between 2D beam and the closest <100> direction, Figure 7d (left).[232] Figure 7d (right) shows nano-spring structures of Si_3N_4 formed using FIB.[233] Helices with different pitches, diameters, chirality, and axes can be patterned by tuning ion beam intensity, time, and irradiation area.[234,233]

3.3. Buckled Ribbons and Membranes

Implementation of residual stress and selective bonding to a soft substrate creates buckling configuration that offers marked

 © 2021 Wiley-VCH GmbH

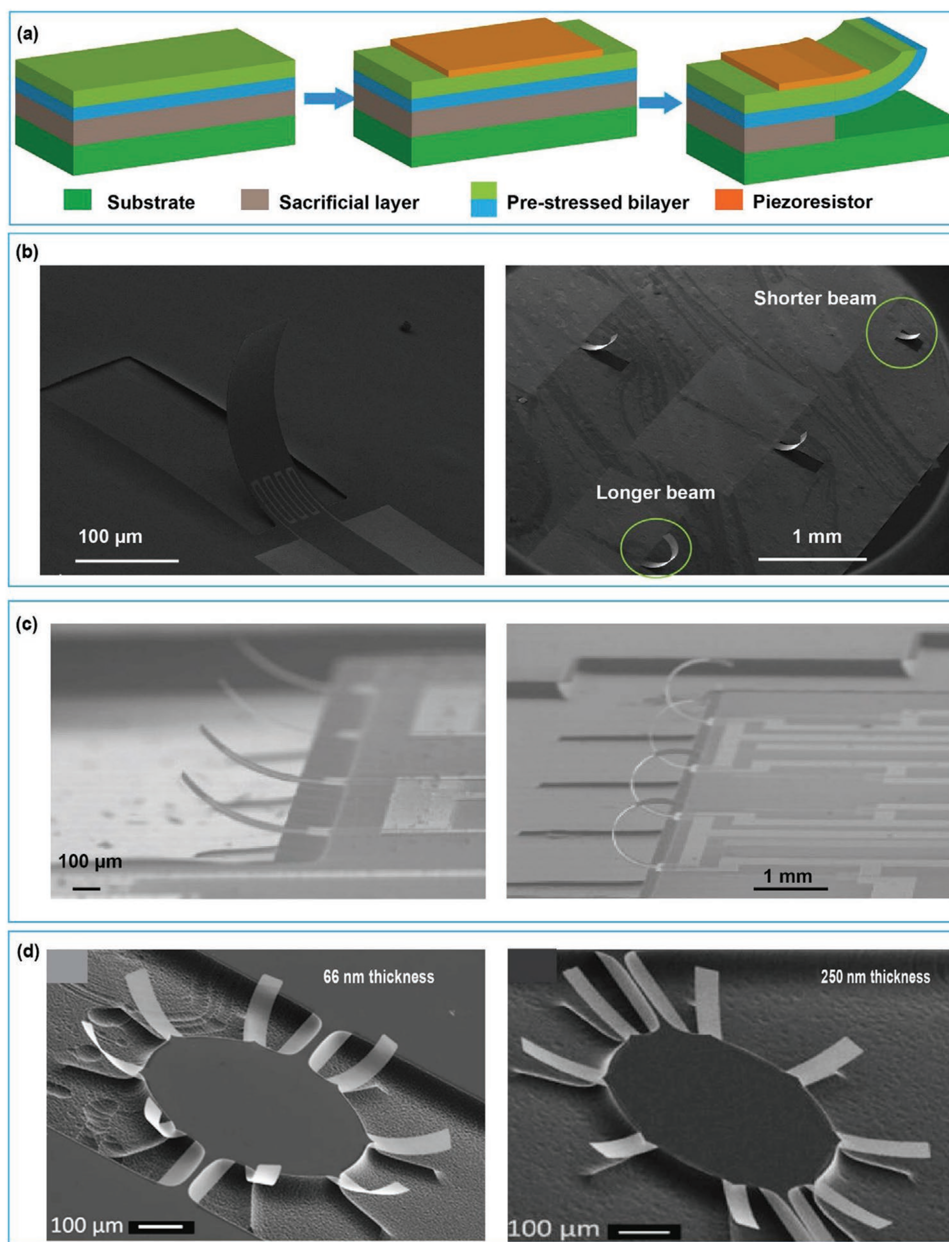

Figure 6. Out-of-plane structure: a) fabrication process of out-of–plane structure; b) SEM images of a single AlN/Mo cantilever (left) and AlN/Mo cantilever array with various lengths (right). Reproduced with permission.[197] Copyright 2011, Elsevier; c) SEM images of Silicon dioxide piezoresistive cantilever beam arrays of 100 µm (left) and 400 µm(right) length. Reproduced with permission.[198] Copyright 2011, Elsevier; d) SEM images SiC curved cantilevers with different thickness. Reproduced with permission.[199] Copyright 2015, AIP Publishing.

benefit to stretchable electronics.[236,237] Functional devices employing buckling structures enable large compression or elongation, with minimal strain induced into the pop-up components. Common buckling structures include wavy structures and island-bridge structures.

The pre-strain approach is widely used to form wavy structures, in which the silicone elastomer substrate undergoes surface treatment (e.g., UV/ozone exposure or oxygen plasma) to activate selective bonding sites and enhance bonding strength. The bonding sites can be either the whole precursor to form the full bonding strategy[152,238,239] (**Figure 8**a (left)) or at the desired areas to form the selective bonding strategy,[240] Figure 8a (middle). The island bridge concept includes functional components firmly bonded to a soft substrate and interconnected via resemble wavy bridges that allow for large deformation, Figure 8a (left).[241] Engineering interconnect bridges using different architectures such as arced shapes,[241,242] serpentines,[243–245] spirals,[246–249] and helices[250–252] can further improve stretchability in functional devices. For instance, arced shapes are generated form straight 2D lines, while helical interconnect are formed from 2D serpentines, Figure 8b.[253] Encapsulating these wave interconnectors can protect devices from

 © 2021 Wiley-VCH GmbH

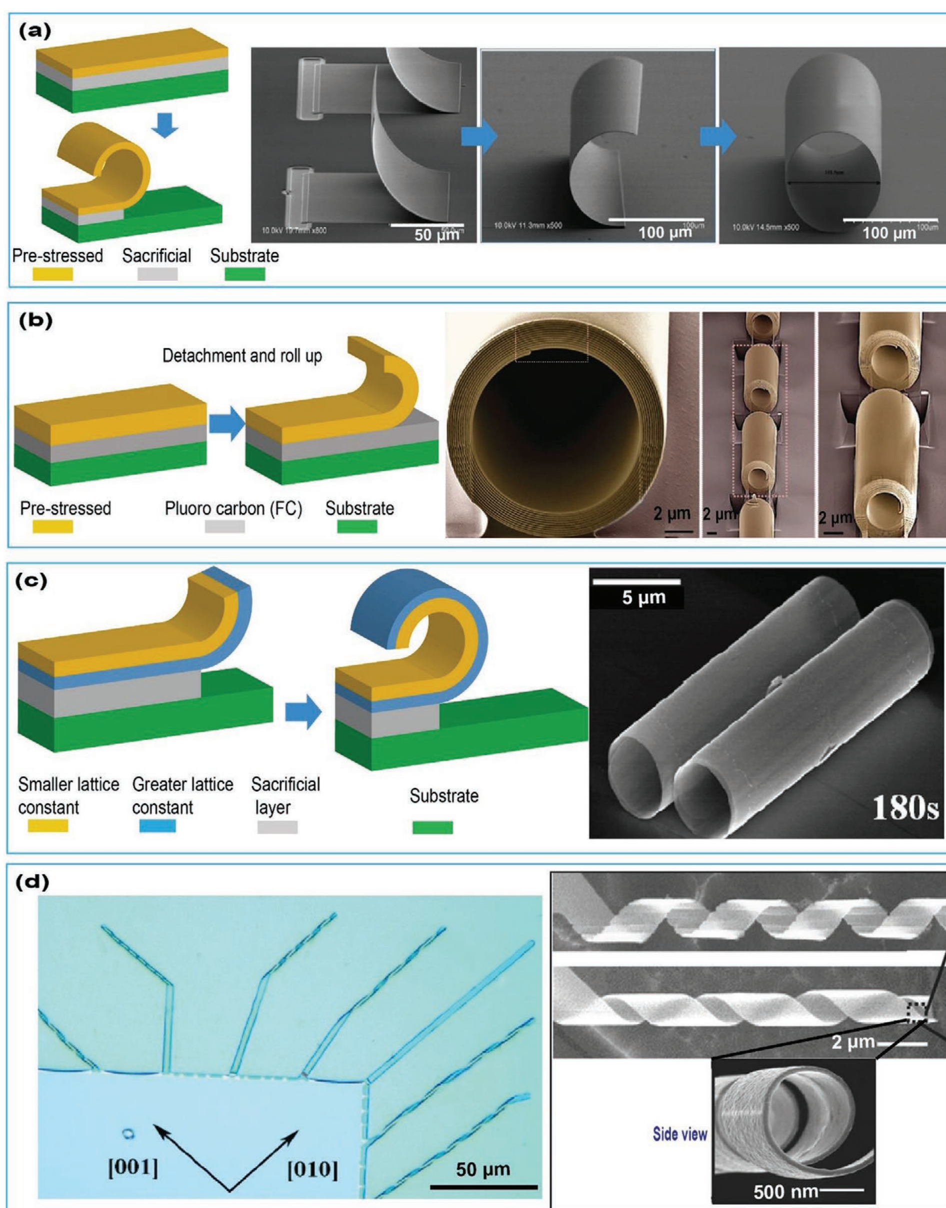

Figure 7. Fabrication of micro/nano tubes and helices: a) Schematic illustration for fabrication principle of nanotube using growth stress and SEM images of 3 different roll up stage of a SiN_x nanotube fabricated base on this method.). Reproduced with permission.[235] Copyright 2014, American Chemical Society; b) schematic illustration of fabrication principle of dry FC-assisted rolling approach, and SEM image of a symmetric and tight rolled-up microtube consisting of $Ti/Cr/Al_2O_3/Cr/Al_2O_3$ layers and 13 rotations fabricated base on this method (scale bars 2 µm.). Reproduced with permission.[224] Copyright 2020, John Wiley and Sons; c) schematic illustration for fabrication principle of nanotube using epitaxial stress and SEM images of $In_{0.3}Ga_{0.7}As$/ GaAs tubes fabricated base on this method.). Reproduced with permission.[225] Copyright 2010, American Chemical Society; d) digital microscope images of helix structures fabricated base on epitaxial stress of InGaAs/GaAs bilayers (left). Reproduced with permission.[232] Copyright 2006, American Chemical Society, and SEM images of helix structures fabricated base on FIB induced stress (right). Reproduced with permission.[233] Copyright 2017, John Wiley and Sons.

surrounding environments (e.g., moisture or corrosion).[254] For instance, Xu et al. developed a packaging method which contains a supporting surface and an encapsulation layer, Figure 8c.[254] These two layers are bonded together, forming a microfluidic reservoir for filling of dielectric fluid to protect the devices. Li et al. proposed a two-stage encapsulation, where substrate with 3D structures were pre-stretched (stage 1), followed by bonding to an encapsulation layer (stage 2).[251] This approach significantly increased stretchability in different interconnectors (e.g., 6× for 2D serpentines, 4× for 2D fractal structure, and 2.6× for 3D helices), Figure 8d.[251]

Beside buckling strain, the residual stress resulted from lattice mismatch was also utilized to create wavy structures. An example of this approach is the InGaAs wavy configuration, Figure 8e.[237] The InGaAs layer was sandwiched between two AlAs sacrificial layers. These triple layers were grown on

© 2021 Wiley-VCH GmbH

NANO · MICRO small
www.small-journal.com

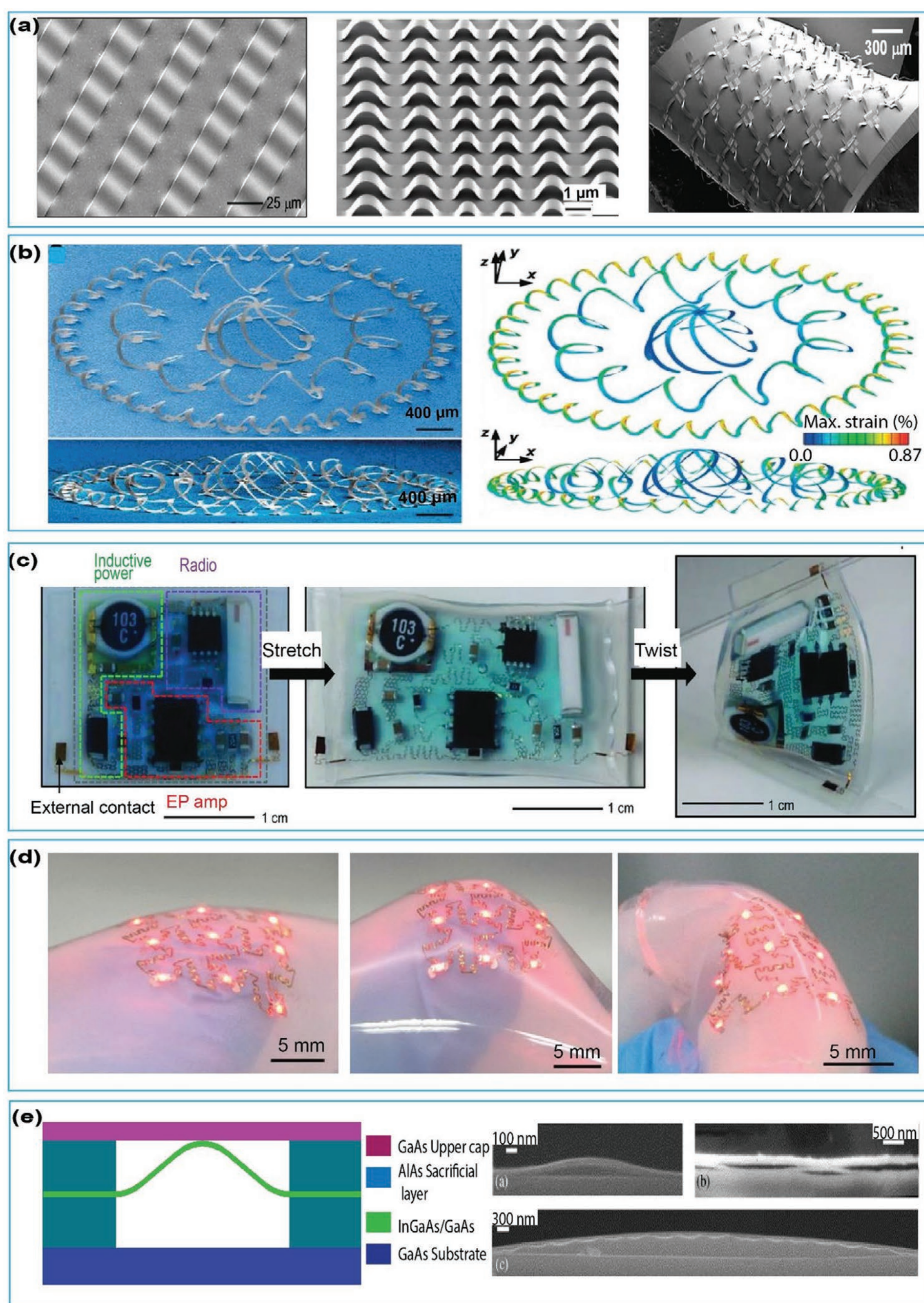

Figure 8. Buckling structures: a) Buckling structure fabricated base on buckling approach: (left) SEM image of fully bonded Si ribbon wavy structure on PDMS substrate. Reproduced with permission.[152] Copyright 2006, AAAS, (middle) SEM images of selectively bonded Si precursors on PDMS substrate. Reproduced with permission.[240] Copyright 2006, Springer Nature BV, (right) SEM image of an island-bridge interconnect. Reproduced with permission.[241] Copyright 2008, PNAS; b) SEM images and FEA predictions of a complex 3D Si mesostructure with helical interconnects. Reproduced with permission.[253] Copyright 2015, AAAS; c) images of a stretchable electronics system that integrate electronics components into a thin elastomer microfluidic enclosure. Reproduced with permission.[254] Copyright 2014, AAAS; d) optical images of a skin-mounted devices which bases on two-stage encapsulation strategy. Reproduced with permission.[251] Copyright 2019, John Wiley and Sons; e) schematic illustration and SEM images of buckled InGaAs-GaAs structures fabricated base on lattice-mismatch stress. Reproduced with permission.[237] Copyright 2024, Elsevier.

a GaAs substrate with another GaAs capping layer on top. Upon removal of the sacrificial layer (AlAs), the InGaAs film buckled up into a wavy pattern due to the epitaxial stress. The magnitude and wavelength can be controlled by increasing or decreasing the gap between the capping layer and the substrate.

3.4. Origami/Kirigami-Inspired 3D Structures

Origami and Kirigami are ancient Japanese art of transforming 2D paper sheets into 3D structures. While Origami only contains a set of folding techniques,[255] Kirigami needs

 © 2021 Wiley-VCH GmbH

both cutting and folding. In the microscale, 2D precursors are formed using micro and nanomachining techniques. Stress engineering such as thermal stress, epitaxial growth, FIB irradiation and buckling stress helps transforming these 2D precursors into 3D Origami and Kirigami configurations.[28]

Figure 9a illustrates an example of micro Origami using residual thermal stress in Cr/Cu bi-layers and Cr/Cu/Cr tri-layer.[256] The Cr/Cu bilayer can bend inward due to the large tensile stress in Cr film, while the Cr/Au/Cr tri-layer can bend outward due to a higher tensile stress in the Cr outer layer. For

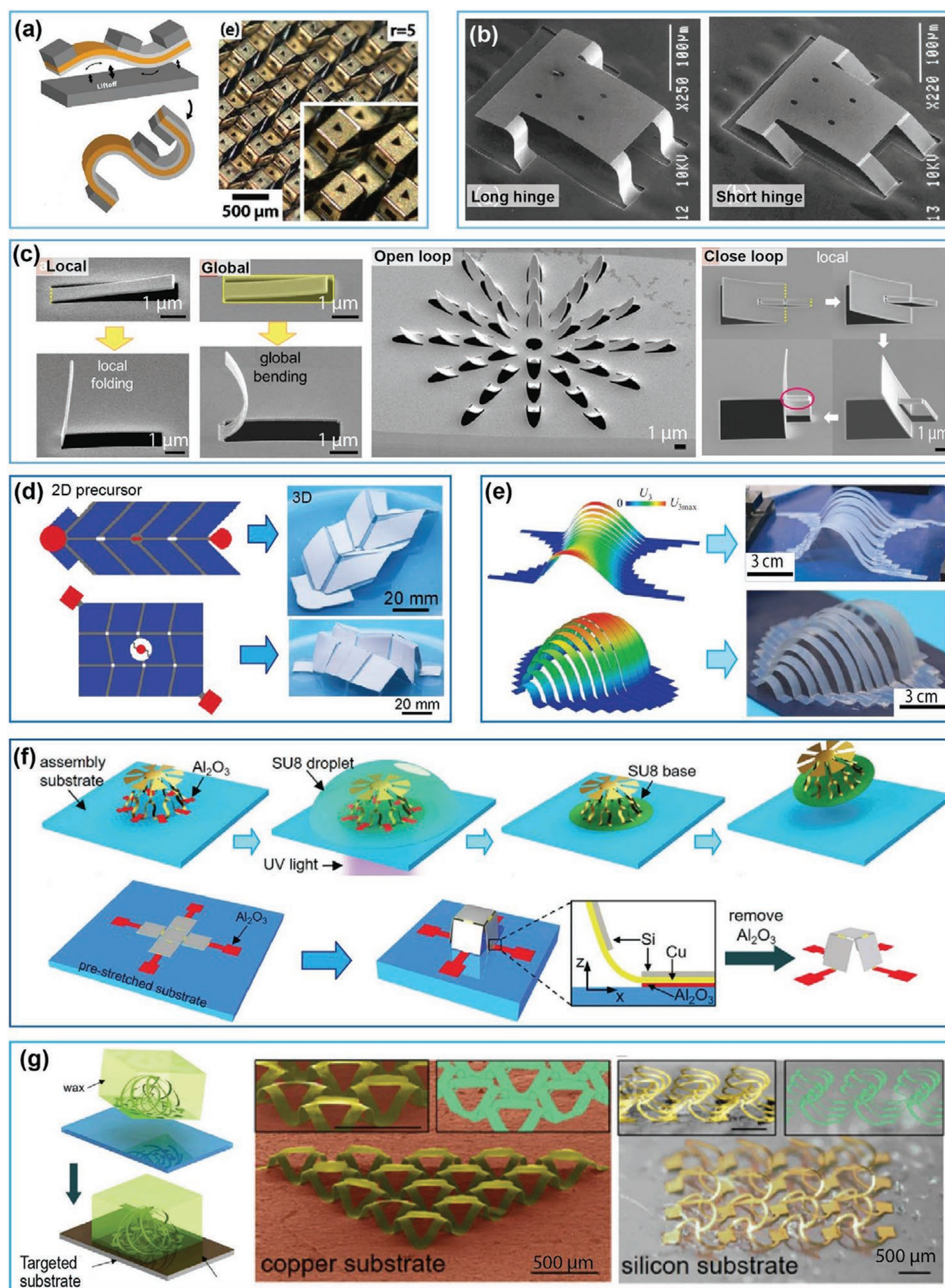

Figure 9. Origami/Kirigami inspired structure: a) origami structure fabricated by engineering growth stress: schematic (left) and optical images of fabricated structure (right). Reproduced with permission.[256] Copyright 2009, AIP Publishing; b) Origami structure fabricated by epitaxy stress: SEM images of two different hinge length showing mountain fold and valley fold. Reproduced with permission.[257] Copyright 2003, Elsevier; c) SEM images of FIB-based Kirigami: i) local irradiation ii) global irradiation iii) tree type Origami iv) close loop Kirigami. Reproduced with permission.[272] Copyright 2018, AIP Publishing; d) Origami fabricated by buckling approach: Optical images of Miura origami (scale bar 1 µm). Reproduced with permission.[273] Copyright 2016, John Wiley and Sons; e) inverse design strategy baseed on theoretical analysis and FEA. Reproduced with permission.[279] Copyright 2020, John Wiley and Sons; f) forming freestanding 3D mesostructures: (up) using wax (down) using plasticity deformation of copper g) transfer 3D structures from soft substrate to targeted substrate (scale bar 500 µm). f,g) Reproduced with permission.[280] Copyright 2017, PNAS.

 © 2021 Wiley-VCH GmbH

areas where bending is not desired, a thick Ni film capped by Au was deposited to enhance the mechanical stiffness. The thickness of Cr and Cu films decide the bending angle of the structure. For example, only a certain thickness combination of those three layers can bend the beam to exactly 90°.

The epitaxial stress has been widely applied to fold 3D Origami and Kirigami from 2D configurations. Vaccaro et al. developed valley-fold or mountain-fold features using two strained layers of $In_{0.19}Ga_{0.81}As$ at the top and GaAs at the bottom.[257] The difference in the lattice constants in these films triggered the bending of the $In_{0.19}Ga_{0.81}As$/GaAs film upward or downward, creating valley folds or mountain folds, Figure 9b.

FIB-based Kirigami is a powerful approach to create complex 3D shapes as it is compatible with a free-standing single layer and only requires a few fabrication steps,[66,141,143,233,258–271] Controlling the parameters of ion beams and the design of 2D precursors can generate a wide variety of 3D structures. For instance, irradiating ion beams locally or to the entire cantilever generates different behaviors of bending. While local irradiation triggers the rigid bending about the irradiated line, full irradiation generates a relatively uniform folding along the longitudinal direction of the cantilever, resulting in a curvature shape, Figure 9c (left).[272] The FIB approach is capable of producing several compelling features such as bending, folding and twisting. For instance, FIB Kirigami using tree-type concept generates 3D configurations, where each joint can bend independently, Figure 9c (middle).[272] On the other hand, in the close-loop procedure, the motion of some subunits can trigger the movement of neighboring objects due to their mechanical constrains, Figure 9c (right).[272] This feature makes the closed loop types resemble to the traditional Kirigami in which only a mechanical trigger can form complicated 3D structures.

Figure 9d shows an example of complex 3D Origami/Kirigami using buckling stress which is called Miura-ori.[273] The buckling method is applicable for configurations with sizes ranging from nanometers up to centimeters.[274] It is also compatible with numerous materials, such as metals, polymers, and semiconductors.[59] These structures require inverse designs using Origami algorithms[275] or lattice Kirigami methods[276–278] to define corresponding 2D patterns for targeted 3D structures. In some case, numerical simulation can accurately predict the 3D structures from a pre-designed 2D precursors with a relevant pre-strain. For instance, Fan et al. used spatial distribution of thickness as a key parameter to precisely produce the desired 3D shapes based on an finite element analysis (FEA) model, Figure 9e.[279]

3D Origami/Kirigami structures formed using buckling can be detached or transferred onto different substrates to further advance their applications. For instance, UV curable polymer can help transferring 3D structures, by simply drop-casting onto targeted 3D Origami/Kirigami, followed by photopolymerization, mechanical detaching, and polymer removal, Figure 9f (up).[280] UV curable gel can be replaced by wax, in which wax functions as an encapsulation layer, allowing the removal of the substrate without altering the embedded 3D shapes. Dissolving wax in a solution releases the original 3D configurations. Alternative method employs the plasticity of metal precursor (e.g., Cu) to keep the original 3D structure without attached to substrate, Figure 9f (down).[280] To avoid spring back effect in metals, FEA methods have been widely employed to optimize the plastic deformation of metals. The final route is inspired by 2D transfer-printing techniques. The 3D mesostructure is embedded in wax encapsulates, which allows removing the substrate without altering the 3D shape. This encapsulated 3D shape is then bonded to a target substrate which is coated with a thin adhesive layer. Finally, the wax is dissolved. The process is shown in Figure 9g.[280]

3.5. Stimuli-Responsive Materials

Self-responsive material offers unconventional routs to form complex architectures via external chemical or physical stimulation. **Figure 10**a shows a bird-like shape of cross linkable SU-8 films which can reversibly flatten or fold into a 3D shape by de-solvation in water.[169] This interesting approach enables the fabrication of bimorph structures, in which functional layers are attached to SU-8 to pop up into desired shapes. An example for this method is a bilayer of graphene and SU-8, with excellent optical transparency for fluorescent applications, Figure 10b.[281]

Other techniques such as electron irradiation, thermal excitation, photon illumination, and chemical absorption have demonstrated their effectiveness in creating 3D configurations. Figure 10c shows SEM images of a poly(methyl methacrylate) (PMMA) butterfly,[165] which was formed using stress generated from electron irradiation. The shape is reconfigurable by controlling irradiation locations the dose of electron beam. 3D structures can also be thermally triggered, as demonstrated in trilayers of photo-crosslinkable copolymers with a temperature-sensitive hydrogel at the middle[162] (Figure 10d). Figure 10e,f present other approaches such as irradiating laser light on GaAs to form 3D mirror arrays[282] (Figure 10e), and activating the chemical reaction in polymer/Cu/Cr layers[283] (Figure 10f) to reversibly switch between 2D and 3D structures. However, it should be noted that the self-assembly approach also possesses several drawbacks. Similar to the reverse design in origami/kirigami, the determination of folding sequences in self-responsive materials remaining a great challenge, which requires further studies to develop complex configurations.[162]

4. Applications of 3D Micro/Nanostructures for MEMS/NEMS Devices

Applications of 3D micro/nanostructures fabricated using stress-based methods can be found in sensors, optical systems, bioelectronics interfaces, micro robots, and implantable and wearable devices with several advantages over 2D configurations. For example, 3D structures that represent the natural architectures of organs and bio tissues are promising candidate for tissue engineering, and fundamental studies of biological systems. Sensors integrated into a 3D layout can possess more functionalities and offer better performance that the 2D counterparts. Implementation of 3D concept has also gained significant interest for optoelectronics, including multifold Fano resonances and optical chirality.

© 2021 Wiley-VCH GmbH

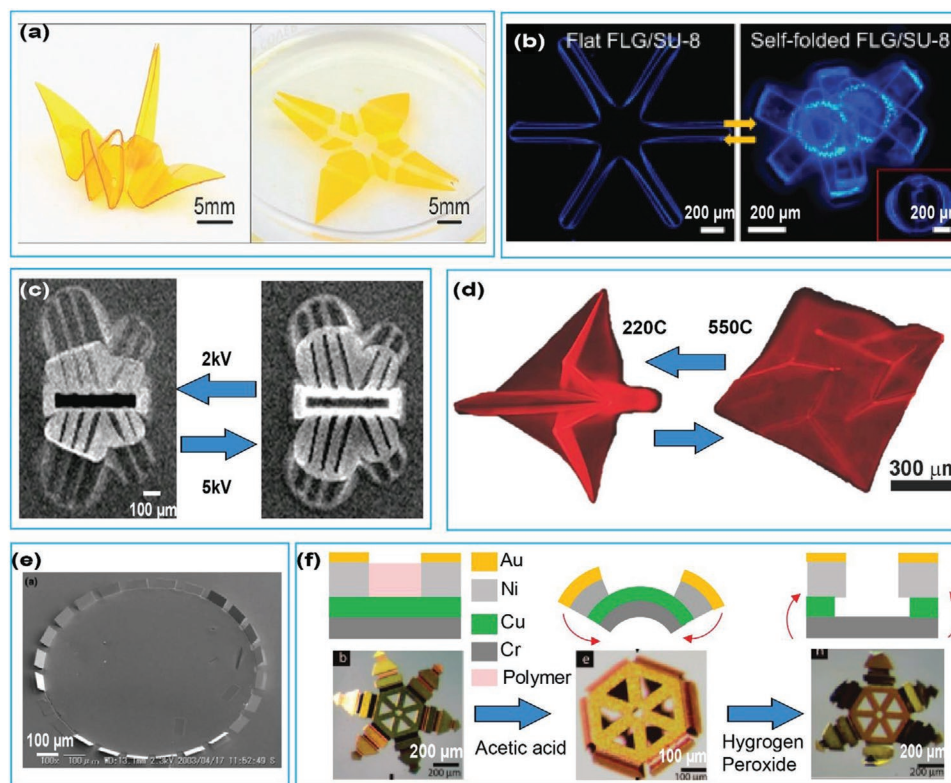

Figure 10. 3D structures from stimuli-response materials: a) Images of self-folded origami structure of SU-8 material. Reproduced with permission.[169] Copyright 2016, John Wiley and Son; b) optical microscope images of self-folding and flattening of a flower shaped FLG/SU-8 structure. Reproduced with permission.[281] Copyright 2015, AIP Publishing; c) SEM images of reversible butterfly PMMA pattern. Reproduced with permission.[165] Copyright 2021, American Chemical Society; d) Thermal actuation of self-folding origami. Reproduced with permission.[162] Copyright 2014, John Wiley and Sons; e) SEM image of a ring of micro-mirrors. Reproduced with permission.[282] Copyright 2014, John Wiley and Sons. f) Schematic illustration and optical microscopy images of a chemically actuated microgripper. Reproduced with permission.[283] Copyright 2008, American Chemical Society.

4.1. Physical Sensors

4.1.1. Flow Sensors

Nature offers several promising approaches for the designing of sensors. Millions years of evolution creates various organs, and body parts of living beings that are simple to imitate, and possess the excellent sensing capability.[284]

The artificial hair cells (AHC) residing in lateral line neuromasts of fishes are highly sensitive to fluidic pressures and flows.[197,201] Inspired by the concept of AHC, several out-of-plane cantilevers have been fabricated for liquid and air flow measurement.[197,198,201,205,207–210,285,286] **Figure 11**a shows a piezoresistive flow sensor made of SiN/Si bilayer.[201] The SiN/Si cantilever was coated by parylene for waterproof, and can function in both air and water environments. Furthermore, using cantilevers facing at different orientations allows for quantification of flow directions. For instance, Abels et al. utilized antiparallel cantilevers for sensing of bidirectional flow. The sensor exhibited superior response under various airflow velocity in two opposite directions compared to single cantilever, Figure 11b.[285]

In 3D MEMS flow sensors, capacitive[287] and piezoresistive effects[197,201,210] effects are most commonly employed due to the ease of their integration capability and associated readout circuits. Capacitive airflow sensors employ out-of-plane cantilevers as movable electrodes, and the substrate as fixed electrodes. The incident flow pushes the cantilevers downward, leading to an increase in the capacitance as the gap between the two electrode is reduced. The capacitance change can be detected from the variation in the resonant frequency of a CMOS ring oscillator integrated with the capacitor. Although this configuration is compatible with numerous conductive materials, it is relatively sensitive to parasitic capacitances.[287] Piezoresistive flow sensors, on the other hand, utilize the change in electrical conductivity under mechanical impacts as the sensing principle and can eliminate the noise from parasitic capacitances. A simpler readout circuit using Wheatstone bridge is another advantage of the piezoresistive effect over the capacitive counterpart. However, piezoresistive sensors are typically sensitive to the variation of surrounding temperatures; therefore, thermal compensation is generally required.

As well as AHC, whiskers that can be found in many insects and mammals have also inspired many researchers to develop soft, multimodal sensors. For instance, Reader et al. introduced electronic whiskers base on shape memory polymer (SMP) that can sense various signals such as temperature, surface roughness, and force, Figure 11c.[288] Furthermore, the use of SMP as the constructing material offer these e-whisker devices the ability to reconfigure their 3D architectures. Specifically, each cantilever of the whisker array can tune its out-of-plane angle to optimize sensing modalities of interest.

© 2021 Wiley-VCH GmbH

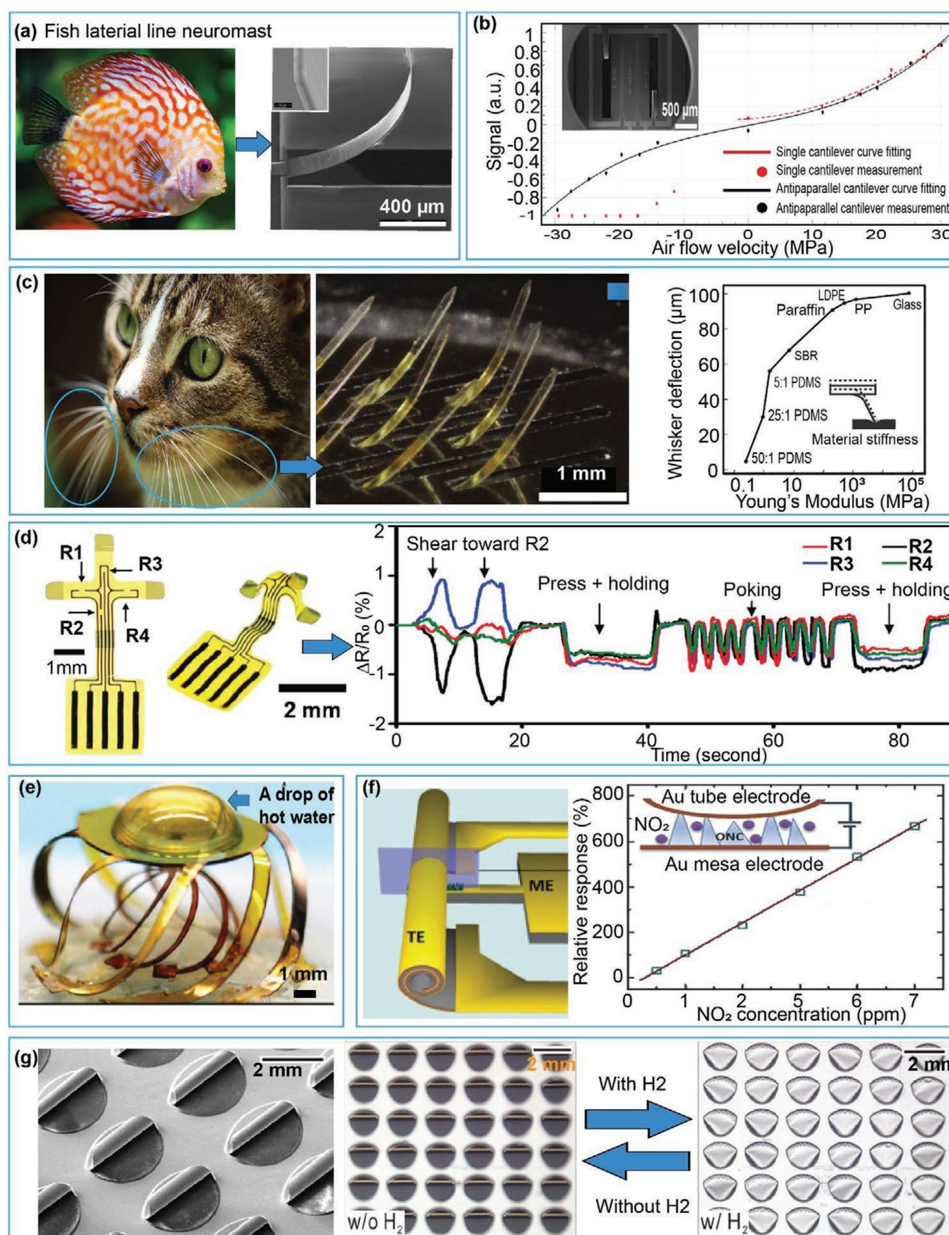

Figure 11. Application of 3D structures in sensor devices: a) flow sensor inspired by fish lateral line neuralmast: SEM of a water proof flow sensor which is coated by parylene. Reproduced with permission.[201] Copyright 2012, Elsevier. Fish image (https://pixabay.com/photos/discus-fish-fish-aquarium-fauna-1943755/); b) bidirectional flow sensor. Reproduced with permission.[285] Copyright 2019, Beilstein Institute for the Advancement of Chemical Sciences; c) electronic whisker of SMP. Reproduced with permission.[288] Copyright 2018, John Wiley and Sons. Cat image (https://pixabay.com/photos/cat-mackerel-domestic-animal-4438600/); d) optical image of 2D precursor with four piezoresistors and 3D piezoresistive sensors, and wirelessly recorded sensing data show responses to shear force and normal pressure. Reproduced with permission.[290] Copyright 2019, American Chemical Society; e) optical image of a table-like shape multifunctional sensor. Reproduced with permission.[291] Copyright 2021, IOP Publishing; f) schematic and conceptual picture of cross section of VOPc based tubular sensor to detect NO_2, and response of sensor to various NO_2 concentration. Reproduced with permission.[292] Copyright 2016, John Wiley and Sons; g) SEM and optical images of Ti/Cr/ Pd gas sensor array for hydrogen detection. Reproduced with permission.[64] Copyright 2018 the authors, AAAS.

4.1.2. Tactile Sensors

Measurement of contacting forces is critically important in robotics and haptic control systems. Strain sensing elements distributed in a 3D hierarchical shape can detect both shear forces and normal pressures, providing valuable feedback signals for robotic control (e.g., grasping objects).[289] Won et al. proposed a multimodal 3D piezoresistive tactile sensor fabricated using the buckling approach, Figure 11d.[290] The sensor is capable of simultaneously measuring multiple mechanical stimuli, such as normal force, shear force, and bending, along with temperature. The tactile sensor utilizes four Si-nanomembrane (NM)

 © 2021 Wiley-VCH GmbH

piezoresistors transferred from an SOI (i.e., silicon on insulator) wafer onto patterned films of PI. Releasing the pre-strains in the PI precursors resulted in a table-like shape, where the four piezoresistive NMs are located at the supporting legs. Normal pressures and shear forces bend the four supporting legs in different directions, leading different patterns of resistance change in the NMs. The buckling structure of the tactile sensors enables excellent flexibility, mechanical reliability, and capability of collapse prevention. Inspired by *Enhydra lutris*, Cheng et al. introduced a multilayer cage-shaped sensor which can monitor the compressive forces and temperatures simultaneously, Figure 11e.[291] This sensor consists of small cages located inside super cage allowing the ability of collapse prevention.

4.1.3. Gas Sensors

Tubular structures have been widely employed in gas sensors due to their large surface-to-volume ratio that enables a high sensitivity and fast recovery.[292] Jalil et al. designed a tubular sensor for detecting NO_2, Figure 11f.[292] The tubular sensor has a layer of vanadyl phthalocyanine (VOPc), which is sandwiched between an Au mesa electrode at the bottom and the Au tube electrode on top. The sensor operates based on the generation of charge carriers through the redox process between phthalocyanine VOPc and NO_2 molecules, which results in the increase of thin film conductivity. Replacing Au by SnO_2 in the tubular structure offers gas sensors with capability of detecting acetone with fast response and high sensitivity.[293] Tubular shapes have also been deployed in hydrogen gas sensors due to their large interface area with surrounding environment, Figure 11g.[64] The sensor contains three layers of titanium (Ti), chromium (Cr), and palladium (Pd) on a glass substrate. Ti/Cr servers as a strained layer while the Pd layer can roll and unroll the tubular structure. This roll and unroll mechanism stems from the fact that tensile strain in the Pd layer can be enhanced or lessen due to the absorption and desorption of hydrogen atoms. This configuration offers several advantages such as rapid response and recovery time, good reversibility, and the capability to integrate high density 3D sensing elements into a device or a system.

4.2. Optical Applications

Several micro/nano-3D structures possess unique optical properties for metal materials and photonic crystals [28,294–296] For example, 3D tubular shape have been utilized in quantum well infrared (IR) photodetectors (QWIP), **Figure 12**a.[297] This 3D tubular QWIP device presents almost an incident angle–independent and wavelength-independent blackbody responsivity with omnidirectional detection under a wide incident angle of ±70°. These interesting features were realized due to the capability to confine the light along the tube wall, which is not possible with the standard planar configurations.[298–300] This light confinement effect generates the whispering mode (WGM) resonance as a result of constructive interference of light traveling along the tube wall. Furthermore, Yin et al. generated plasmonic silver nanoparticles on nanotubes cavity to studied the photon-plasmon coupling, Figure 12b.[301] This coupling effect could be adjusted by changing the size, morphology, and location of nanoparticle spots on the tube cavity.

Another representative example of 3D optical devices is Fano resonance with potential applications in biosensing, optical imaging, and optical wave guides.[269] Using the FIB induced stress method, Cui et al.[268] investigated the optical performances of a U-type plasmonic nanograters array. The device consists of vertical U-shape split-ring resonators (SRR) located along the edge of horizontal subwavelength rectangular holes, that exhibited scalable unusual Fano resonances, Figure 12c. Liu et al. demonstrated the same Fano resonances although their structural geometries were largely different from the work reported by Cui and colleagues.[269] Modulating the symmetric U-shape split-ring by asymmetric designs results in double Rabi splitting in triple Fano resonances.[266] Furthermore, 3D metamaterial consisting of two asymmetric plates at two parallel edges of a rectangular hole can produce fivefold Fano resonances under linearly polarized light incidence.[259] These results suggest a promising pathway to engineer Fano resonances by designing 3D structures.

Close-loop Kirigami has demonstrated interesting photonic applications, including 3D twisting hierarchal shapes for giant intrinsic optical chirality.[66] Due to the twisted loop in all directions, electric and magnetic fields of the incident light could induce electric and magnetic moments in the parallel direction. As a result, 3D pinwheel structures exhibit circular dichroism (CD) and polarization rotation angle under normal incidences, which are not observed in 2D platforms, Figure 12d.[66] Interestingly, CD spectra of left-handed (LH) and right-handed (RH) configurations show nearly opposite signs with similar amplitudes. Furthermore, modifying the number of arms in pinwheel structures can change its intrinsic optical property.[302] The utilization of 3D Archimedean spiral structures can enhance broadband near-field optical chirality in the infrared regime with extraordinary chiral dissymmetry in the transmission.[303] The 3D pinwheel-like structure was also used to investigate polarization conversion and phase engineering in metasurfaces.[142,272] For example, pattern of this structure with opposite handedness with an appropriate periodicity L can diffract the incident light in different patterns depending on their wavelength. According to diffraction theory, when L is smaller than wavelength λ, the y-polarized light will be diffracted by an angle α that satisfies $L \sin \alpha = (m-1/2)\lambda$ (i.e., m can be 1 or 0), while the x-polarized light will not change its incident direction. As shown in Figure 12e, where $L = 1.45$ µm and $\lambda = 1.68$ µm, most of the light is converted into the diffracted beams with y-polarization.[272] In contrast, at 1.2-µm wavelength, only the center spot is observed as the cross-polarized transmission is nearly zero. Furthermore, LH and RH 3D pinwheel-like structures arranged alternatively in a radial direction showed an interesting diffraction pattern, Figure 12f.[272] The circularly polarized light can be diffracted into a spot at the center or outer rings depending on the polarization of the incident light. These results showed that pinwheel-like structures with suitable patterns can diffract both linearly polarized incidence and circularly polarized light.[272] These 3D micro pinwheels can be fabricated using FIB or the buckling method,[158] Figure 12g.[158]

 © 2021 Wiley-VCH GmbH

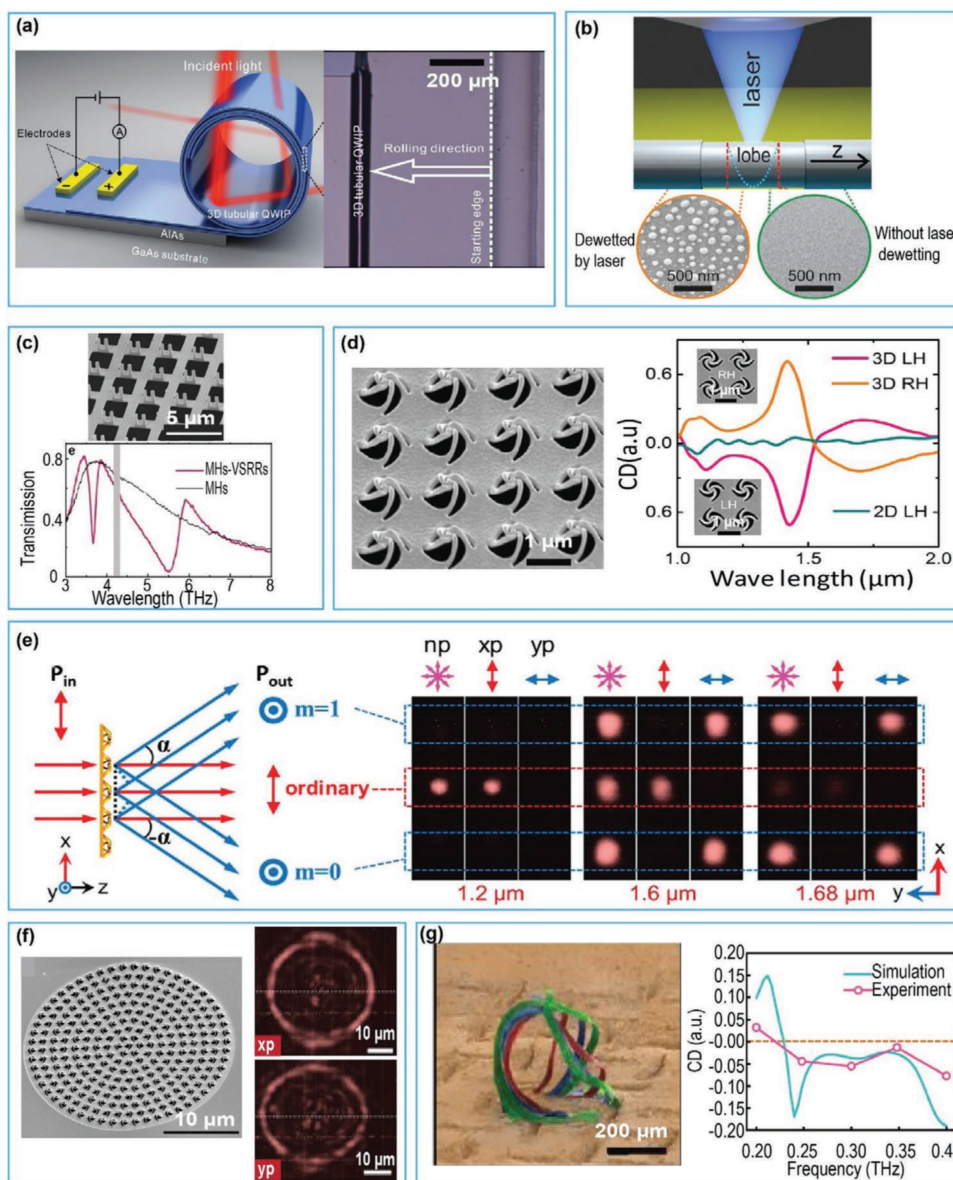

Figure 12. Application of 3D structures in optical devices: a) schematic diagram and optical image for 3D tubular QWIP. Reproduced with permission.[297] Copyright 2016, The Authors, Published by AAAS; b) schematic illustration of the laser-induced dewetting to generate silver nanoparticles on nanotube cavity, and SEM images shows the irradiated region with nanoparticle, and the nonirradiated area without nanoparticles. Reproduced with permission.[301] Copyright 2018, American Chemical Society; c) SEM images of U-shape split ring resonator (SRR) with Fano resonances. Reproduced with permission.[268] Copyright 2015, Springer Nature; d) SEM image of 3D pin wheel arrays with left hand (LH) and right hand (RH) arrays and their CD transmission spectrum. Reproduced with permission.[66] Copyright 2018, Copyright AAAS; e) schematic illustration of diffraction properties, and CCD camera images of light spots of various wave length. Reproduced with permission.[272] Copyright 2018, AIP Publishing; f) SEM images of a circular nanograter and tis CCD camera images of transmitted light with *xp* and *yp* detections under *x*-polarized incidence at wavelength o 1.55 nm. Reproduced with permission.[272] Copyright 2018, AIP Publishing; g) SEM images of a 3D morphable multilayered microstructures as mechanically tunable optical chiral metal-materials and its measured and simulated optical CD. Reproduced with permission.[158] Copyright 2019, PNAS.

4.3. Bioelectronic Interfaces

Tissue engineering (TE) is a recent and promising field which potentially offers a solution for the repairing and generation of tissues and damaged organs.[304] TE aims to solve the drawbacks of conventional treatment based on organ transplants by using cells, scaffolds, and bioactive factors to restore, nurture, improve the function of living organs or tissues.[304] Three key factors of TE are cells, scaffolds, and bioelectronics interface. The scaffolds work as extracellular matrix providing support for cell attachment and tissue generation. Extracellular matrix (ECM) is where most of cells in human body locate in. Scaffolds should mimic the real shapes, structures, functions, and biomechanics of ECM. To achieve that purpose, scaffolds need to satisfy a number of requirements on architecture, biocompatibility, bioactivity, and mechanical integrity[24,305,306] Surfaces

of scaffolds should enhance the attachment of cells and tissues while the 3D structures and volume of scaffolds should provide enough space for the proliferation, and remodeling of cells and tissues. In terms of bioactivity, scaffolds should be able to deliver growth-stimulating signal to make tissues growth faster as well as record the growth signal, and rehabilitation signal of tissues. In fact, 2D structures are unable to satisfy those basic requirements and is being replace by 3D scaffolds.

An example of scaffolds for in vitro studies of living cell behaviors is the use of micro tubes made from SiO_2 and Al_2O_3, **Figure 13**a.[307] In this work, Yeast cells were seeded to study growth behavior of cells within tubes of various diameters.

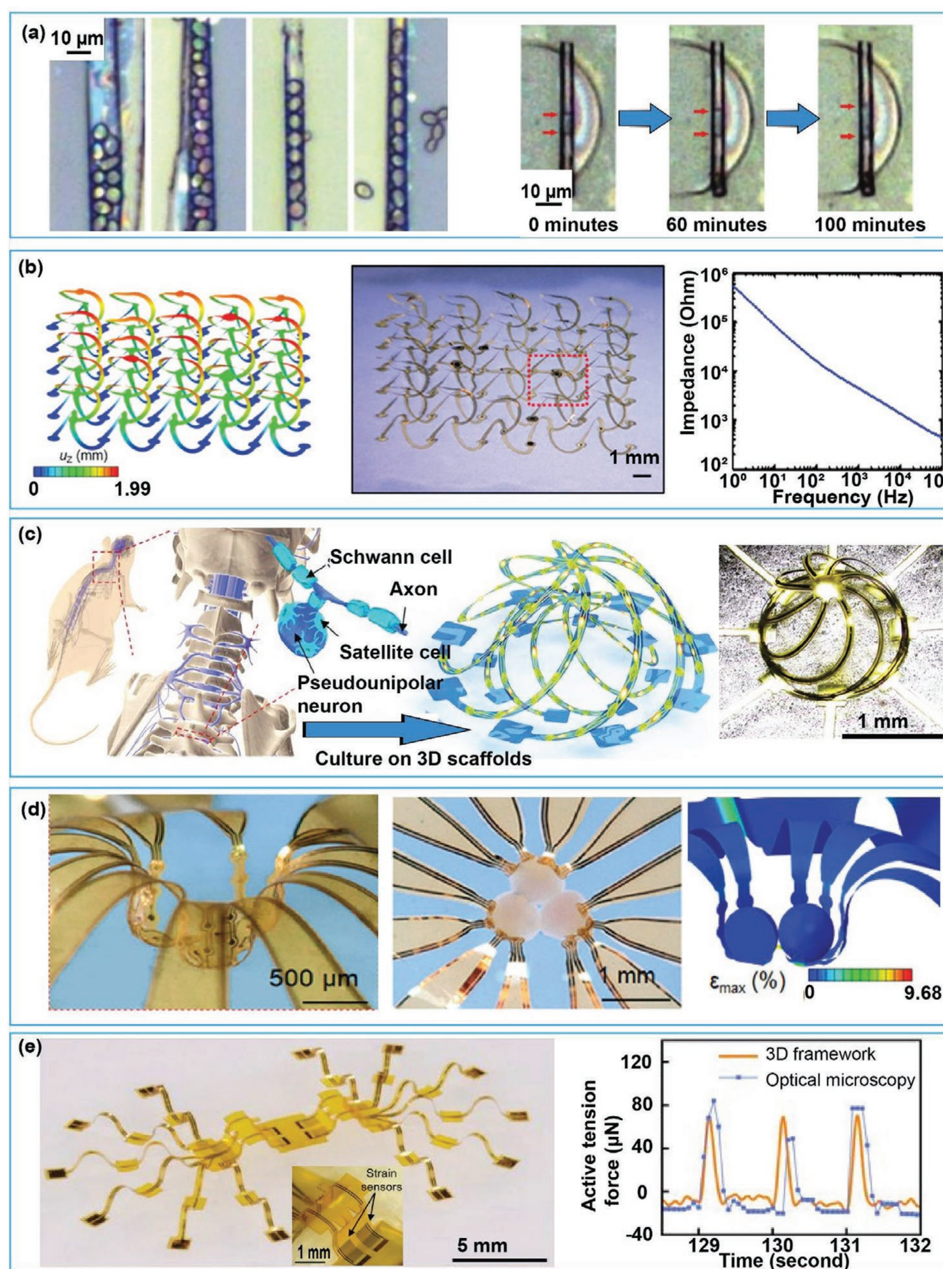

Figure 13. Application of 3D structures in cell scaffolds and engineering tissues: a) optical microscope images of four different microtubes containing yeast cells with tube diameters decrease from left to right, and optical image yeast cell growth in a micro tube, the red marks showed the size of developed yeast cells. Reproduced with permission.[307] Copyright 2001, Royal Society of Chemistry; b) FEA modeling, optical images of 3D electronic scaffolds of a 3D lectronics scaffolds, and its impedance characterization in cell culture medium. Reproduced with permission.[309] Copyright 2020, Elsevier; c) schematic illustration of rat dorsal root ganglion (DRG) and the cell populations within them, schematic illustration and SEM image of a representative electrode. Reproduced with permission,[280] Copyright 2017, PNAS; d) optical images of 3D MMF designed to create assembloids of three spheroids in a triangular lattice geometry and the FEA results of the structure. Reproduced with permission.[65] Copyright 2021, The Authors, Published by AAAS. e) Optical images of a spider-like scaffold (left) and a comparison of the measured active tension force between the spider-like frame work and the optical microscopy (right). Reproduced with permission.[312] Copyright 2021, PNAS.

© 2021 Wiley-VCH GmbH

Interestingly, depending on the diameter of the tubes, cells can grow in different patterns such as zigzag chains or a single column. The results revealed that the expansion and proliferation of cells can be engineered using 3D geometrical constrains. Furthermore, transparent tubes offer quantum well photo detecting effects, thereby suggesting a promising possibility of simultaneous cell observation and optical analysis.

Electronics integrated into 3D scaffolds have also been used for electrical stimulation and evaluation of drug delivery.[308] **Figure 14**b shows an example of 3D scaffolds.[309] In these devices, micro electrodes distributed in 3D offers capability to control cardiac tissues' growth and at the same time monitor the electrical activities of the engineered tissues. Furthermore, by positively charging the polypyrrole deposited on conductive surface of electrodes and negatively charging the drug molecules, these functional 3D scaffolds can release drug on demand through the reduction of polymer film that breaks the electrostatic bonds. This concept provides a new route to understand the efficacy of selected drugs. A similar approach was employed to study more complex biosystems such as engineered neural tissues.[310] For instance, the 3D bilayers nested cages of epoxy which are able to guide the growth of dorsal root ganglion (DRG) cells, Figure 13c.[280] Implementing these 3D structures with electrodes allows probing the electrophysiological behaviors of growing DRG neural networks. This study could pave the way for the application in human neural system in the future.

3D multielectrode array (MEAs) offer compliant, multifunctional neural interfaces to organ-like systems such as spheroids and assembloids.[311,65] These 3D devices with low bending

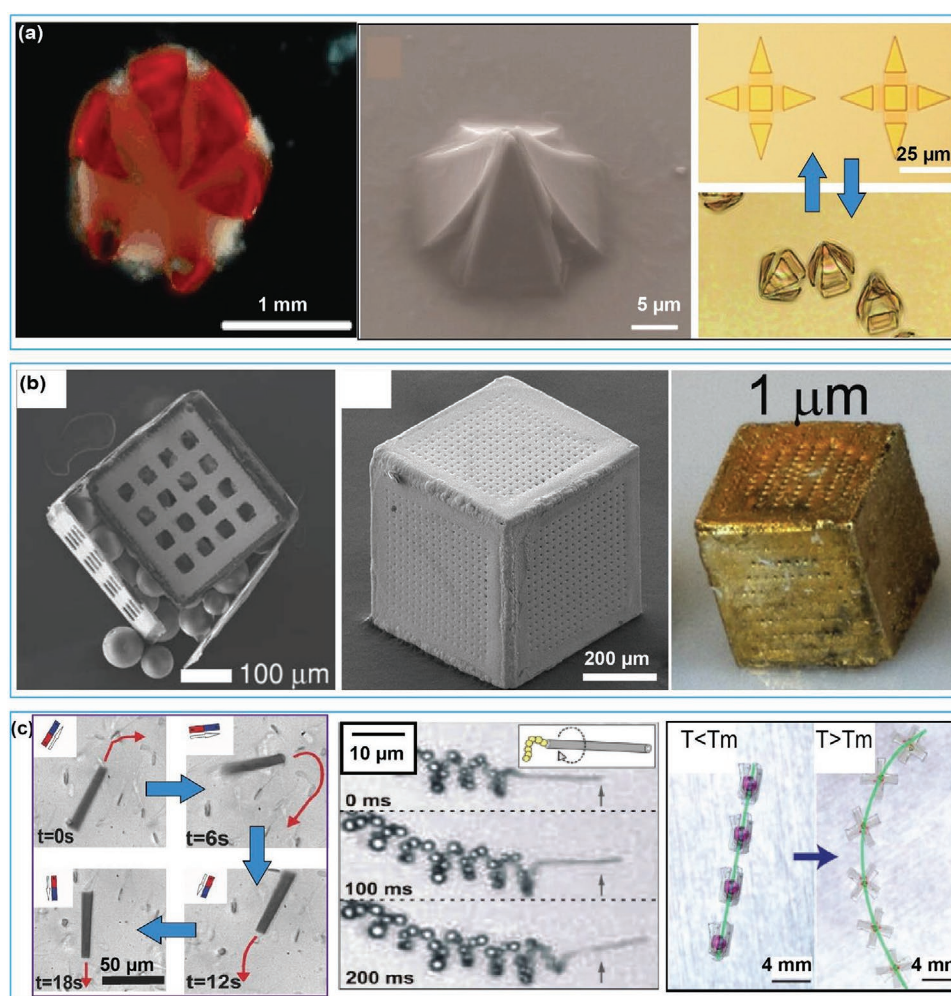

Figure 14. Application of 3D structures in micro/nanoactuator and robot: a) microgrippers: (left) optical image of micro-gripper griping a clump of cell. Reproduced with permission.[316] Copyright 2014, John Wiley and Sons, (middle) SEM image of a closed single cell grippers of SiO/SiO_2 bilayers, (right) optical images of 50 µm grippers of SiO/SiO_2 bilayers in open and close state. Middle and right are reproduced with permission.[315] Copyright 2014, American Chemical Society; b) micro self container: (left) SEM image of self-loaded microcontainer overfilled with glass beads. Reproduced with permission.[62] Copyright 2014, Royal Society of Chemistry, (middle) SEM image of porous microcontainer, (right) image of Au-coated 1-µm-sized container. Reproduced with permission.[320] Copyright 2014, Royal Society of Chemistry; c) micro robots: (left) SEM image of a sperm driven microrobot. Reproduced with permission.[319] Copyright 2013, John Wiley and Sons. (middle) images of a self-proplled nanojet. Reproduced with permission.[322] Copyright 2012, American Chemical Society, (right) two different trajectories of micro robot under different temperature. Reproduced with permission.[170] Copyright 2019, John Wiley and Sons.

 © 2021 Wiley-VCH GmbH

stiffness and have the capability to wrap and hold multiple neural spheroids, Figure 13d. At the same time, they can support multifunctional devices including electrodes, sensors, and modulators on their individual wings. These new functions strongly unpin fundamental studies of the growth, transection, and regrowth of neurite bridges between these spheroids, as a way to model neural injuries and recovery. Another promising candidate for studying tissues disease and drug screening is the spider-like configuration as shown in Figure 13e, establishing an compliant interfaces with engineered muscle tissues such as muscle rings, Figure 13e (right).[312] In the spider-like structure, four resistive strain sensors with a half attached to the substrate and a half buckled up creating a roof-like region. This configuration is highly sensitive to the horizontal forces, thus offering the mechanotransdution sensing capability. The spiker-like sensor showed better performances compared to conventional optical microscopy especially at high sampling rate. Furthermore, the open architecture of this 3D structure combining with the on-chip sensing capabilities also offers opportunities to study the effect of drugs on skeletal muscles.

4.4. Micro Robots, Micro/Nanoactuators

Residual stress in thin films provide novel approaches for developing micro/nanoactuators,[313–317] and micro/nanorobots.[318,319] Figure 14a shows examples of micro grippers operating based on thermal induced stress.[316] These grippers consist of flexible, thermally responsive hinges and rigid patterns. The actuators capture cells and living tissues or even deliver drugs. Microcontainer is a powerful tool to encapsulate living (such as cells) and non-living (such as drug molecules) objects, Figure 14b (left).[62] Microcontainers provide channel to cell to cell interaction, transplant xenogeneic, allogeneic, or stem cells. Furthermore, using stress-driven assembly approach, microcontainers can load to the 3D cubic or unload into the cruciform under the outside stimuli such as temperature. One more underlying advantages of microcontainers is that the well-designed porous structures can allow selective nutrients and therapeutics moving inside while block the immune components of the host bodies, Figure 14b (middle, right).[320] Microcontainers, therefore, are potential candidates for cell transplantation.

Combining 3D architectures with living tissues generates a new class of robots, namely cyborg such as a sperm-driven micro robot. One example of microrobots is the sperm cell trapped into a micro tube made of titanium and iron, Figure 14c (left).[319] Sperm cells act as a micro motor while the micro tube is a controller which guides the moving direction of the robot using an external magnet. This robot has potential to deliver sperm cells to desired egg cells, Figure 14c (left). Chemical reactions that generate micro and nanobubbles have also been utilized in robots working in liquid environments, namely microswimmers.[321] For instance, roll-up InGaAs/GaAs/Cr/Pt multilayer nanomembranes works as a bubble-driven catalytic nanojet in of hydrogen peroxide (H_2O_2) solution, Figure 14c (middle). The Pt layer functions as the catalyst for the decomposition reaction of hydrogen peroxide into water and oxygen. In a more complex design, Pt is coupled with shape memory polymers (SMPs) to form a self-propeller.[170] The robot can transform between folded and unfolded shapes as a result of changing its ambient temperature around the melting point of the SMPs. This unique feature leads to different strategies of motion and the potential for the capture and release of small objects. Figure 14c (right) illustrates two different trajectories of the micro robot under different temperatures. When temperature is below melting temperature (Tm), the planar robots fold and wrap the object inside, while the robots unfold into turbine shape as temperature increase above Tm. This turbine shape allows multidirectional gas generation which create the circular trajectory.

4.5. Flexible, Wearable, and Implantable Electronics

3D micro/nanostructures offer a promising future for flexible electronic devices since their geometries are stretchable, and reconfigurable. A potential application using 3D structures is electrically small antennas (ESA). **Figure 15**a shows a 3D meander-shaped hemispherical ESA (MHESA) and a helix-based hemispherical ESA (HHESA).[322] These ESAs showed the ability to accommodate large deformation. They also showed tunable working frequencies and sustainability under extreme mechanical deformation. While 2D ESAs have several limitation about efficiencies and bandwidth, 3D ESAs become the future of small antennas with the capabilities to sustainably improve their performances.[322] The ability to transform between 3D and 2D shapes offer additional functionalities in electronics devices. Figure 15b shows an example of a photodetector with integrated electrodes.[323] The folded cubic shape increased optical absorption significantly compared to 2D cruciform MoS2 array. Furthermore, the large surface area in several microscale and nanoscale 3D structures have also ben tailored for the development of energy harvesting and storage devices.[324–327] For example, Lee et al. introduced a nano-biocapacitor (nSBCs) which can withstand external forces from blood flow and muscle contraction due to the “Swiss-roll” shape, Figure 15c.[325] The devices can self-charge energy by employing bio-electrocatalytic reactions between redox enzymes and living cells in blood charges. The proton exchange separator layer in this Swiss-roll SBC prevents the self-discharge due to side redox reaction. Experimental results demonstrated a self-charge voltage of ≈1 V when operate in blood and can well function for over 5000 charge–discharge cycles. This miniaturized, biocompatible, and self-charged device suggests a promising research direction for implantable robots that can access to regions deep inside the human body.

The stretchability of 3D micro/nanostructures allows electronic devices to function reliably even under extreme mechanic conditions.[250,328] From this super properties, several implantable and wearable devices which can be comfortably mounted onto skin to monitor parameters relevant to physiological status and biomechanics of soft tissues have been introduced.[329–335] These devices are miniature, ultra-low modulus, and biocompatible to living tissues. The structures allow devices not only to deform following the conformal shape of the interested areas in the body but also to support a wide range of continuous motions across different regions of the body during natural movement[336,337] One example of 3D implantable devices

 © 2021 Wiley-VCH GmbH

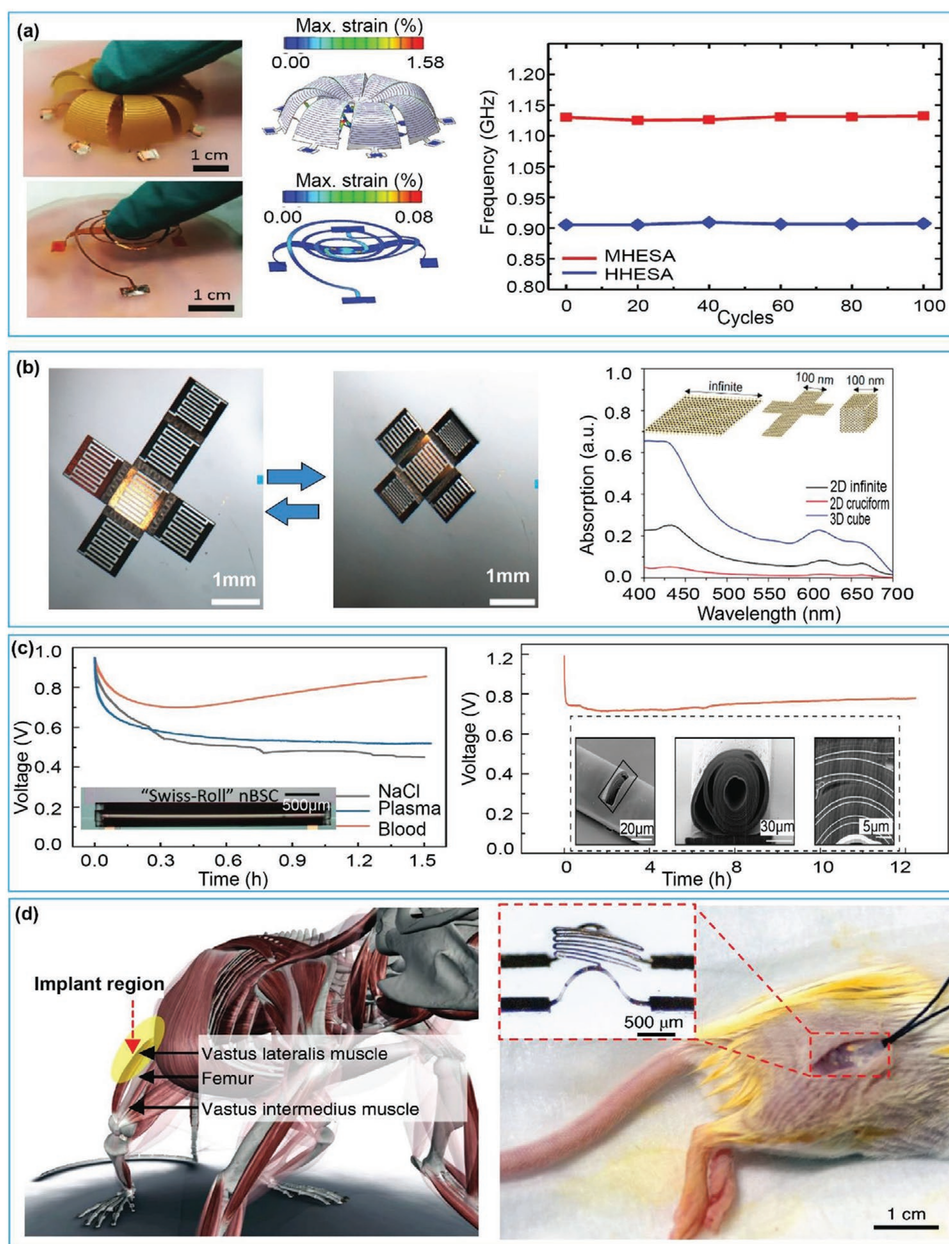

Figure 15. Application of 3D structures in flexible, wearable, and implantable electronic devices: a) optical image and FEA results of MHESA and HHESA. Reproduced with permission.[322] Copyright 2018, John Wiley and Sons; b) image of a MoS2–Au–SU8 photodetector from their 2D precursors. Reproduced with permission.[323] Copyright 2019, American Chemical Society; c) nanobiosupercapacitor can self-charge in blood for short time (left) and after galvanostatic charge-discharge 5000 cycles (right). Reproduced with permission.[325] Copyright 2021, Springer Nature; d) a 3D subdermal implant and its implanted locations. Reproduced with permission.[63] Copyright 2019, Springer Nature.

is the 3D compliant piezoelectric micro system as shown in Figure 15d.[63] This 3D structure with low stiffness is able to deform follow the motions of surrounding muscles, thus producing repeatable, stronger, and more stable output signals.

5. Conclusion and Perspective

Strain engineering represents powerful approaches for the formation of several unusual 3D micro and nanoarchitectures, opening a frontier area for fundamental and applied research in multidiscipline of bioelectronics, robotics, optoelectronics, and sensing. Compared to other techniques, stress-based approaches possess several key advantages including suitability for a wide range of materials, fabrication scalability from a single component to arrays of devices, and feasibility to form complex geometries.

Strain engineering offer multiple pathways to generate stress in thin films, providing versatile routes to fabricate different types of 3D structures. Among these, methods that use

 © 2021 Wiley-VCH GmbH

intrinsic stress and epitaxy stress are promising for wafer-scale-level development of 3D designs. However, as these stresses are influenced by numerous parameters such as thermal coefficients of expansion, lattice constants, and the density of defects, the principles of these stress are not fully understood and utilized. Some existing theoretical models which partly explain the principles of stress in thin films are only applicable under certain conditions and assumptions. A universal model, which can fully describe the stress behaviors of thin films, would allow for accurate prediction of the 3D geometry either in simulations or through theoretical analysis. This will require further theoretical and experimental studies to elucidate and employ the concept of growth stresses for the development of complex structures. Stress induced from micro processing (e.g., ion implantation, pre-strain on substrates, and stimuli-induced stress) have emerged as strong candidates for well-controlled and reconfigurable architectures. These stresses are typically combined with open-loop or close-loop methods to generate different hierarchical structures. Common structures employed process-induced stress include cantilevers, table-shapes, 3D spirals, and buckled serpentines. Although fabricated 3D shapes are increasingly complex, they are still limited to relatively simple shapes with limited applications. Moreover, to produce these 3D shapes through engineering stress approaches to industrial productions, inverse design problems must be addressed. That is, given a desired 3D shape, a 2D precursor and a suitable fabrication process must be designed to meet the requirements. Inverse design methods of 3D shapes, however, are still in a premature state. Therefore, further development in advanced computational and numerical analysis for complex 3D structures can be anticipated in the coming years. Another technical challenge is the design of simple but effective methods to transfer the as-fabricated devices onto or into working or functioning substrates/environments without shape-distortion and performance-degradation.

3D architectures can be found in numerous applications such as strain sensing, optical filters, wearable/implantable devices, and bioelectronics interfaces. For sensing application, the use of 3D structures where sensing elements are distributed in different locations enables the measurement of physical parameters (e.g., flow, force) in all *XYZ* directions (e.g., shear force and normal pressure in tactile sensors). These features advance several industrial monitoring systems (e.g., flow direction monitoring) and robotic controls (e.g., gripping control and haptic control). Some technical issues require further design optimization, including reduction of crosstalk and repeatability. For optical devices, 3D configurations offer breakthrough concepts such as Fano resonance and optical chirality. A combination of these 3D configurations with micro actuation methods (e.g., electrostatic or electromagnetic forces) can modify the initial shapes, enabling enhancement in broadband wavelengths as well as tunability in transmission spectrum. Flexible electronics in the form of wearable and implantable devices are anticipated as one of the major technologies in the MedTech sector. In fact, some wearable devices have been successfully translated into commercial products including smart pads for heartbeat and respiration monitoring, and UV dosimeters. Although significant progress has been made in wearable technologies, further development is required to enhance reliability and durability. Integration of multimodal components in a single wearable device to monitor different biophysiological signals from users along with implementation of wireless technologies for direct data transmission to healthcare providers is of significant interest. For implanted devices, 3D architectures are expected to effectively support cell growth through their unique scaffold network or electrical stimulation. These features are one of the most exciting technologies for medical devices, particularly for the treatment of neuron disorders and cardiovascular diseases. Extensive investigations using in vitro (e.g., organ on chips), in vivo (e.g., animal studies) models and clinical trials are imperative to validate these emerging technologies. A promising technique for in vitro studies is the implementation of 3D electronics scaffolds where integrated functional elements form conformal contacts with 3D biological tissues such as organoids. 3D bioelectronic interfaces can monitor a range of biophysiological signals and at the same time trigger electrical stimulation, underpinning the investigation into complex neuron systems as well as the development of neuron diseases. With these compelling functionalities, progress in strain engineering in thin films for 3D architectures could expand capabilities and opportunities in the highly interdisciplinary area of materials, electronics, optics, and biology.

Conflict of Interest

The authors declare no conflict of interest.

Keywords

flexible electronics, micro-/nano-3D structures, stress, thin films

Received: September 20, 2021
Revised: October 23, 2021
Published online: December 7, 2021

[1] J. J. Vlassak, *Int. J. Fract.* **2003**, *120*, 299.
[2] J. L. Beuth, *Int. J. Solids Struct.* **1991**, *29*, 1657.
[3] E. G. L. R. F. Cook, *J. Electrochem. Soc.* **1999**, *146*, 4439.
[4] M. George, C. Coupeau, J. Colin, J. Grilhé, *Acta Mater.* **2005**, *53*, 411.
[5] J. Liu, S. Kou, *Acta Mater.* **2017**, *125*, 513.
[6] H. Li, D. Gao, S. Xie, J. Zou, *Sci. Rep.* **2016**, *6*, 36451.
[7] Z. Peng, C. Wang, L. Chen, S. Chen, *Int. J. Solids Struct.* **2014**, *51*, 4596.
[8] J. Y. Faou, G. Parry, S. Grachev, E. Barthel, *Phys. Rev. Lett.* **2012**, *108*, 116102.
[9] G. Parry, A. Cimetière, C. Coupeau, J. Colin, J. Grilhé, *Phys. Rev. E* **2006**, *74*, 066601.
[10] F. Jean-Yvon, S. Grachev, E. Barthel, G. Parry, *Acta Mater.* **2017**, *125*, 524.
[11] R. Boijoux, G. Parry, J. Y. Faou, C. Coupeau, *Appl. Phys. Lett.* **2017**, *110*, 141602.
[12] R. A. J. M. J. M. van den Bos, J. Reinink, D. V. Lopaev, C. J. Lee, J. P. H. H. Benschop, F. Bijkerk, *J. Phys. D. Appl. Phys.* **2018**, *51*, 115302.
[13] B. Yuan, C. M. Harvey, G. W. Critchlow, R. C. Thomson, S. Wang, *Mater. Des. Process. Commun.* **2019**, *1*, e60.
[14] H. D. Espinosa, B. C. Prorok, M. Fischer, *J. Mech. Phys. Solids* **2003**, *51*, 47.

© 2021 Wiley-VCH GmbH

[15] S. E. Thompson, M. Armstrong, C. Auth, M. Alavi, M. Buehler, R. Chau, S. Cea, T. Ghani, G. Glass, T. Hoffman, C. H. Jan, C. Kenyon, J. Klaus, K. Kuhn, Z. Ma, B. Mcintyre, K. Mistry, A. Murthy, B. Obradovic, R. Nagisetty, P. Nguyen, S. Sivakumar, R. Shaheed, L. Shifren, B. Tufts, S. Tyagi, M. Bohr, Y. El-Mansy, *IEEE Trans. Electron Dev.* **2004**, *51*, 1790.
[16] S. Thompson, N. Anand, M. Armstrong, C. Auth, B. Arcot, M. Alavi, P. Bai, J. Bielefeld, R. Bigwood, J. Brandenburg, M. Buehler, S. Cea, V. Chikarmane, C. Choi, R. Frankovic, T. Ghani, G. Glass, W. Han, T. Hoffmann, M. Hussein, P. Jacob, A. Jain, C. Jan, S. Joshi, C. Kenyon, J. Klaus, S. Klopcic, J. Luce, Z. Ma, B. McIntyre, K. Mistry, A. Murthy, P. Nguyen, H. Pearson, T. Sandford, R. Schweinfurth, R. Shaheed, S. Sivakumar, M. Taylor, B. Tufts, C. Wallace, P. Wang, C. Weber, M. Bohr, Digest International Electron Devices Meet, IEEE, San Francisco, CA **2002**, pp. 61–64.
[17] S. E. Thompson, M. Armstrong, C. Auth, S. Cea, R. Chau, G. Glass, T. Hoffman, J. Klaus, Z. Ma, B. Mcintyre, A. Murthy, B. Obradovic, L. Shifren, S. Sivakumar, S. Tyagi, T. Ghani, K. Mistry, M. Bohr, Y. El-Mansy, *IEEE Electron Device Lett.* **2004**, *25*, 191.
[18] B. S. Kang, S. Kim, J. Kim, F. Ren, K. Baik, S. J. Pearton, B. P. Gila, C. R. Abernathy, C.-C. Pan, G.-T. Chen, J.-I. Chyi, V. Chandrasekaran, M. Sheplak, T. Nishida, S. N. G. Chu, *Appl. Phys. Lett.* **2003**, *83*, 4845.
[19] M. Azize, A. L. Hsu, O. I. Saadat, M. Smith, X. Gao, S. Guo, S. Gradecak, T. Palacios, *IEEE Electron Device Lett.* **2011**, *32*, 1680.
[20] W. C. Cheng, S. Lei, W. Li, F. Zhao, M. Chan, H. Yu, *2019 Electron Devices Technol. Manuf. Conf. EDTM*, IEEE, Singapore **2019**, pp. 374–376.
[21] S. Shervin, S.-H. Kim, M. Asadirad, S. Ravipati, K.-H. Lee, K. Bulashevich, J.-H. Ryou, *Appl. Phys. Lett.* **2015**, *107*, 193504.
[22] T. T. Luong, Y. T. Ho, B. T. Tran, Y. Y. Woong, E. Y. Chang, *Chem. Vap. Depos.* **2015**, *21*, 33.
[23] S. N. Bhatia, D. E. Ingber, *Nat. Biotechnol.* **2014**, *32*, 760.
[24] M. P. Nikolova, M. S. Chavali, *Bioact. Mater.* **2019**, *4*, 271.
[25] V. A. Bolaños Quiñones, H. Zhu, A. A. Solovev, Y. Mei, D. H. Gracias, *Adv. Biosyst.* **2018**, *2*, 1800230.
[26] J. W. Haycock, *Methods Mol. Biol.* **2011**, *695*, 1.
[27] S. Campuzano, A. E. Pelling, *Front. Sustain. Food Syst.* **2019**, *3*, 38.
[28] S. Chen, J. Chen, X. Zhang, Z. Y. Li, J. Li, *Light Sci. Appl.* **2020**, *9*, 2047.
[29] D. A. Pawlak, S. Turczynski, M. Gajc, K. Kolodziejak, R. Diduszko, K. Rozniatowski, J. Smalc, I. Vendik, *Adv. Funct. Mater.* **2010**, *20*, 1116.
[30] C. A. Ross, K. K. Berggren, J. Y. Cheng, Y. S. Jung, J.-B. Chang, *Adv. Mater.* **2014**, *26*, 4386.
[31] S. H. Yoo, H. S. Lee, *Acc. Chem. Res.* **2017**, *50*, 832.
[32] K. Miszta, J. De Graaf, G. Bertoni, D. Dorfs, R. Brescia, S. Marras, L. Ceseracciu, R. Cingolani, R. Van Roij, M. Dijkstra, L. Manna, *Nat. Mater.* **2011**, *10*, 872.
[33] F. Hong, F. Zhang, Y. Liu, H. Yan, *Chem. Rev.* **2017**, *117*, 12584.
[34] K. Yamada, M. Yamada, H. Maki, K. M. Itoh, *Nanotechnology* **2018**, *29*, 28LT01.
[35] M. V. Gorkunov, V. E. Dmitrienko, A. A. Ezhov, V. V. Artemov, O. Y. Rogov, *Sci. Rep.* **2015**, *5*, 9273.
[36] S. G. Park, S. K. Lee, J. H. Moon, S. M. Yang, *Lab Chip* **2009**, *9*, 3144.
[37] Y. Chen, K. Bi, Q. Wang, M. Zheng, Q. Liu, Y. Han, J. Yang, S. Chang, G. Zhang, H. Duan, *ACS Nano* **2016**, *10*, 11228.
[38] M. C. George, E. C. Nelson, J. A. Rogers, P. V. Braun, *Angew. Chem., Int. Ed.* **2009**, *48*, 144.
[39] H. Ning, J. H. Pikul, R. Zhang, X. Li, S. Xu, J. Wang, J. A. Rogers, W. P. King, P. V. Braun, *Proc. Natl. Acad. Sci. U. S. A.* **2015**, *112*, 6573.
[40] J. Park, J. H. Park, E. Kim, C. W. Ahn, H. I. Jang, J. A. Rogers, S. Jeon, *Adv. Mater.* **2011**, *23*, 860.
[41] B. Salhi, D. Troadec, R. Boukherroub, *Nanotechnology* **2017**, *28*, 205301.
[42] S. C. Warren-Smith, R. M. André, C. Perrella, J. Dellith, H. Bartelt, *Opt. Express* **2016**, *24*, 378.
[43] S. Takahashi, K. Suzuki, M. Okano, M. Imada, T. Nakamori, Y. Ota, K. Ishizaki, S. Noda, *Nat. Mater.* **2009**, *8*, 721.
[44] O. J. Hildreth, A. G. Fedorov, C. P. Wong, *ACS Nano* **2012**, *6*, 10004.
[45] N. Chekurov, K. Grigoras, A. Peltonen, S. Franssila, I. Tittonen, *Nanotechnology* **2009**, *20*, 065307.
[46] Y. Zhou, X. Y. Chen, Y. H. Fu, G. Vienne, A. I. Kuznetsov, B. Luk'Yanchuk, *Appl. Phys. Lett.* **2013**, *103*, 123116.
[47] D. C. Meisel, M. Wegener, K. Busch, *Phys. Rev. B – Condens. Matter Mater. Phys.* **2004**, *70*, 165104.
[48] D. J. Shir, S. Jeon, H. Liao, M. Highland, D. G. Cahill, M. F. Su, I. F. El-Kady, C. G. Christodoulou, G. R. Bogart, A. V. Hamza, J. A. Rogers, *J. Phys. Chem. B* **2007**, *111*, 12945.
[49] M. J. Burek, N. P. De Leon, B. J. Shields, B. J. M. Hausmann, Y. Chu, Q. Quan, A. S. Zibrov, H. Park, M. D. Lukin, M. Lončar, *Nano Lett.* **2012**, *12*, 6084.
[50] T. G. Leong, P. A. Lester, T. L. Koh, E. K. Call, D. H. Gracias, *Langmuir* **2007**, *23*, 8747.
[51] J. H. Cho, A. Azam, D. H. Gracias, *Langmuir* **2010**, *26*, 16534.
[52] J. H. Cho, D. H. Gracias, *Nano Lett.* **2009**, *9*, 4049.
[53] Y. Hu, Z. Lao, B. P. Cumming, D. Wu, J. Li, H. Liang, J. Chu, W. Huang, M. Gu, *Proc. Natl. Acad. Sci. U. S. A.* **2015**, *112*, 6876.
[54] J.-H. Cho, M. D. Keung, N. Verellen, L. Lagae, V. V. Moshchalkov, P. Van Dorpe, D. H. Gracias, *Small* **2011**, *7*, 1943.
[55] C. Py, P. Reverdy, L. Doppler, J. Bico, B. Roman, C. N. Baroud, *Phys. Rev. Lett.* **2007**, *98*, 156103.
[56] A. Legrain, T. G. Janson, J. W. Berenschot, L. Abelmann, N. R. Tas, *J. Appl. Phys.* **2014**, *115*, 214905.
[57] J. Wang, M. Patel, D. H. Gracias, *Nano* **2009**, *4*, 1.
[58] X. Cheng, Y. Zhang, *Adv. Mater.* **2019**, *31*, 1901895.
[59] H. Zhao, Y. Lee, M. Han, B. K. Sharma, X. Chen, J. H. Ahn, J. A. Rogers, *Nano Today* **2020**, *30*, 100825.
[60] G. Huang, Y. Mei, *Small* **2018**, *14*, 1703665.
[61] X. Ning, X. Wang, Y. Zhang, X. Yu, D. Choi, N. Zheng, D. S. Kim, Y. Huang, Y. Zhang, J. A. Rogers, *Adv. Mater. Interfaces* **2018**, *5*, 1800284.
[62] T. G. Leong, C. L. Randall, B. R. Benson, A. M. Zarafshar, D. H. Gracias, *Lab Chip* **2008**, *8*, 1621.
[63] M. Han, H. Wang, Y. Yang, C. Liang, W. Bai, Z. Yan, H. Li, Y. Xue, X. Wang, B. Akar, H. Zhao, H. Luan, J. Lim, I. Kandela, G. A. Ameer, Y. Zhang, Y. Huang, J. A. Rogers, *Nat. Electron.* **2019**, *2*, 26.
[64] B. Xu, Z. Tian, J. Wang, H. Han, T. Lee, Y. Mei, *Sci. Adv.* **2018**, *4*, eaap8203.
[65] Y. Park, C. K. Franz, H. Ryu, H. Luan, K. Y. Cotton, J. U. Kim, T. S. Chung, S. Zhao, A. Vazquez-Guardado, D. S. Yang, K. Li, R. Avila, J. K. Phillips, M. J. Quezada, H. Jang, S. S. Kwak, S. M. Won, K. Kwon, H. Jeong, A. J. Bandodkar, M. Han, H. Zhao, G. R. Osher, H. Wang, K. H. Lee, Y. Zhang, Y. Huang, J. D. Finan, J. A. Rogers, *Sci. Adv.* **2021**, *7*, 9153.
[66] Z. Liu, H. Du, J. Li, L. Lu, Z.-Y. Y. Li, N. X. Fang, *Sci. Adv.* **2018**, *4*, eaat4436.
[67] P. J. Withers, H. K. D. H. Bhadeshia, *Mater. Sci. Technol.* **2001**, *17*, 366.
[68] Y. Y. Hu, W. M. Huang, in *Handbook of Manufacturing. Engineering and Technology*, Springer, London **2013**, pp. 1–71.
[69] M. F. Doerner, W. D. Nix, *Crit. Rev. Solid State Mater. Sci.* **1988**, *14*, 225.
[70] B. R. York, *Crit. Rev. Solid State Mater. Sci.* **1995**, *20*, 125.
[71] H. Windischmann, *Crit. Rev. Solid State Mater. Sci.* **1992**, *17*, 547.

© 2021 Wiley-VCH GmbH

[72] G. Abadias, E. Chason, J. Keckes, M. Sebastiani, G. B. Thompson, E. Barthel, G. L. Doll, C. E. Murray, C. H. Stoessel, L. Martinu, *J. Vac. Sci. Technol. A* **2018**, *36*, 020801.
[73] J. A. Thornton, *J. Vac. Sci. Technol.* **1975**, *12*, 830.
[74] R. W. Hoffman, *Thin Solid Films* **1976**, *34*, 185.
[75] E. Klokholm, *J. Vac. Sci. Technol.* **1969**, *6*, 138.
[76] S. D. Dahlgren, W. L. Nicholson, M. D. Merz, W. Bollmann, J. F. Devlin, R. Wang, *Thin Solid Films* **1977**, *40*, 345.
[77] P. V. Plunkett, R. M. Johnson, C. D. Wiseman, *Thin Solid Films* **1979**, *64*, 121.
[78] E. Chason, J. W. Shin, S. J. Hearne, L. B. Freund, *J. Appl. Phys.* **2012**, *111*, 083520.
[79] C. Ayas, E. Van Der Giessen, *Model. Simul. Mater. Sci. Eng.* **2009**, *17*, 064007.
[80] R. Koch, H. Leonhard, R. Abermann, *Thin Solid Films* **1982**, *89*, 117.
[81] P. M. Alexander, R. W. Hoffman, *J. Vac. Sci. Technol.* **1976**, *19*, 96.
[82] L. A. Davis, *Fundamental Aspects of Structural Alloy Design*, Springer US, Boston, MA, **1977**, pp. 431–450.
[83] J. T. Pan, I. Blech, *J. Appl. Phys.* **1984**, *55*, 2874.
[84] H. Horikoshi, N. Tamura, *Jpn. J. Appl. Phys.* **1963**, *2*, 328.
[85] C. Herring, *Phys. Rev.* **1951**, *82*, 87.
[86] R. Shuttleworth, *Proc. Phys. Soc. Sect. A* **1950**, *63*, 444.
[87] J. S. Vermaak, C. W. Mays, D. Kuhlmann-Wilsdorf, *Surf. Sci.* **1968**, *12*, 128.
[88] A. Shintani, S. Sugaki, H. Nakashima, *J. Appl. Phys.* **1980**, *51*, 4197.
[89] E. Chason, P. R. Guduru, *J. Appl. Phys.* **2016**, *119*, 191101.
[90] E. Chason, *Thin Solid Films* **2012**, *526*, 1.
[91] V. Gervilla, G. A. Almyras, B. Lü, K. Sarakinos, *Sci. Rep.* **2020**, *10*, 2031.
[92] E. Chason, J. W. Shin, C. H. Chen, A. M. Engwall, C. M. Miller, S. J. Hearne, L. B. Freund, *J. Appl. Phys.* **2014**, *115*, 123519.
[93] B. W. Sheldon, K. H. A. Lau, A. Rajamani, *J. Appl. Phys.* **2001**, *90*, 5097.
[94] A. M. Engwall, Z. Rao, E. Chason, *Mater. Des.* **2016**, *110*, 616.
[95] R. Abermann, *Vacuum* **1990**, *41*, 1279.
[96] E. Suhir, *J. Appl. Phys.* **2011**, *110*, 074506.
[97] A. Moridi, H. Ruan, L. C. Zhang, M. Liu, *Int. J. Solids Struct.* **2013**, *50*, 3562.
[98] J. Haider, M. Rahman, B. Corcoran, M. S. J. Hashmi, *J. Mater. Process. Technol.* **2005**, *168*, 36.
[99] D. Yang, X. Zhang, J. Zhu, *Surfaces* **2021**, *4*, 89.
[100] G. Schiavone, A. S. Bunting, M. P. Y. Desmulliez, A. J. Walton, *J. Microelectromech. Syst.* **2015**, *24*, 870.
[101] H. Geiler, K. Schulz, R. Knechtel, *Microsystem Technologies*, Springer, Berlin **2013**, pp. 697–703.
[102] Z. Cui, *Encyclopedia of Microfluidics and Nanofluidics*, Springer US, Boston, MA **2008**, pp. 2179–2183.
[103] V. Dragoi, E. Pabo, J. Burggraf, G. Mittendorfer, in *Microsystem Technologies*, Springer, Berlin **2012**, pp. 1065–1075.
[104] V. Dragoi, G. Mittendorfer, J. Burggraf, M. Wimplinger, *ECS Trans.* **2019**, *33*, 27.
[105] H. A. Yang, M. Wu, W. Fang, in Proceedings of IEEE International Conference Micro Electro Mechanical Systems, Maastricht, Netherlands **2004**, pp. 729–732.
[106] G. P. Horn, R. Gerbach, T.-W. Lin, M. Bernach, S. Brand, H. T. Johnson, *ECS Trans.* **2019**, *33*, 553.
[107] J. Wei, H. Xie, M. L. Nai, C. K. Wong, L. C. Lee, *J. Micromech. Microeng.* **2003**, *13*, 217.
[108] R. A. Inzinga, T. W. Lin, M. Yadav, H. T. Johnson, G. P. Horn, *Exp. Mech.* **2012**, *52*, 637.
[109] X. Hu, M. Meng, M. Baeuscher, U. Hansen, S. Maus, O. Gyenge, P. Mackowiak, B. Mukhopadhyay, N. Vokmer, O. Ehrmann, K. Dieter Lang, H. D. Ngo, *Proceedings of 2016 IEEE 18th Electronics Packaging Technology Conference (EPTC)*, Institute Of Electrical And Electronics Engineers Inc., Singapore **2017**, pp. 325–330.
[110] S. Ogawa, M. Imada, S. Noda, *Appl. Phys. Lett.* **2003**, *82*, 3406.
[111] B. W. Lin, N. J. Wu, Y. C. S. Wu, S. C. Hsu, *IEEE/OSA J. Disp. Technol.* **2013**, *9*, 371.
[112] D. Ho, H. Jeong, S. Choi, C. Kim, *J. Mater. Chem. C* **2020**, *8*, 14983.
[113] L. Wan, F. He, Y. Qin, Z. Lin, J. Su, J. Chang, Y. Hao, *Materials (Basel)* **2018**, *11*, 1761.
[114] B. C. Prorok, H. D. Espinosa, *J. Nanosci. Nanotechnol.* **2002**, *2*, 427.
[115] G. Wiederhirn, T. J. Balk, G. Dehm, J. Nucci, G. Richter, E. Arzt, *AIP Conf. Proc.* **2006**, *817*, 185.
[116] D. Gan, P. S. Ho, Y. Pang, R. Huang, J. Leu, J. Maiz, T. Scherban, *J. Mater. Res.* **2006**, *21*, 1512.
[117] R. D. Tenaglia, D. F. Lahrman, *Nat. Photonics* **2009**, *3*, 267.
[118] W. Zhang, Y. L. Yao, I. C. Noyan, *J. Manuf. Sci. Eng. Trans. ASME* **2004**, *126*, 18.
[119] W. Zhang, Y. L. Yao, I. C. Noyan, *J. Manuf. Sci. Eng. Trans. ASME* **2004**, *126*, 10.
[120] Y. Wang, H. Chen, J. W. Kysar, Y. Lawrence Yao, *J. Manuf. Sci. Eng.* **2007**, *129*, 485.
[121] J. A. Fox, *Appl. Phys. Lett.* **1974**, *24*, 461.
[122] C. S. Montross, T. Wei, L. Ye, G. Clark, Y. W. Mai, *Int. J. Fatigue* **2002**, *24*, 1021.
[123] Y. Liao, C. Ye, G. J. Cheng, *Opt. Laser Technol.* **2016**, *78*, 15.
[124] T. Sano, T. Eimura, R. Kashiwabara, T. Matsuda, Y. Isshiki, A. Hirose, *J. Laser Appl.* **2017**, *29*, 012005.
[125] Y. Sagisaka, K. Yamashita, W. Yanagihara, H. Ueta, *J. Mater. Process. Technol.* **2015**, *219*, 230.
[126] Y. Sagisaka, M. Kamiya, M. Matsuda, Y. Ohta, *J. Mater. Process. Technol.* **2010**, *210*, 2304.
[127] B. Sun, H. Qiao, J. Zhao, *AIP Adv.* **2018**, *8*, 095203.
[128] M. S. Amer, L. Dosser, S. LeClair, J. F. Maguire, *Appl. Surf. Sci.* **2002**, *187*, 291.
[129] M. S. Amer, M. A. El-Ashry, L. R. Dosser, K. E. Hix, J. F. Maguire, B. Irwin, *Appl. Surf. Sci.* **2005**, *242*, 162.
[130] Y. R. Kim, P. Chen, M. J. Aziz, D. Branton, J. J. Vlassak, *J. Appl. Phys.* **2006**, *100*, 104322.
[131] N. Teranishi, G. Fuse, M. Sugitani, *Sensors* **2018**, *18*, 2358.
[132] Y. Chen, *Microelectron. Eng.* **2015**, *135*, 57.
[133] C. Li, G. Habler, L. C. Baldwin, R. Abart, *Ultramicroscopy* **2018**, *184*, 310.
[134] T. Goto, F. Imaizumi, S. Sugawa, *IEEE Electron Device Lett.* **2017**, *38*, 345.
[135] A. Guseva, S. Akhmadaliev, J. Bischoff, C. Csato, S. Illhardt, A. Zowalla, M. Rub, in *Proceedings of International Conference on Ion Implantation Technology*, Institute Of Electrical And Electronics Engineers Inc., Piscataway, New Jersey **2018**, pp. 97–100.
[136] V. Sharma, A. Herklotz, T. Z. Ward, F. A. Reboredo, *Sci. Rep.* **2017**, *7*, 11166 .
[137] W. L. Li, W. D. Fei, T. Hanabusa, *Appl. Surf. Sci.* **2006**, *252*, 2847.
[138] K.-W. Weng, Y.-C. Chen, S. Han, C.-S. Hsu, Y.-L. Chen, D.-Y. Wang, *Thin Solid Films* **2007**, *516*, 5330.
[139] C. H. Lin, Z. Pei, S. Maikap, C. C. Wang, C. Sen Lu, L. S. Lee, M. J. Tsai, Y. J. Chan, *Appl. Phys. Lett.* **2005**, *87*, 262109.
[140] M. Liu, H. Ruan, L. Zhang, *J. Mater. Res.* **2013**, *28*, 1413.
[141] W. J. Arora, S. Sijbrandij, L. Stern, J. Notte, H. I. Smith, G. Barbastathis, *J. Vac. Sci. Technol. B* **2007**, *25*, 2184.
[142] J. Li, Z. Liu, *Nanophotonics* **2018**, *7*, 1637.
[143] W. J. Arora, H. I. Smith, G. Barbastathis, *Microelectron. Eng.* **2007**, *84*, 1454.
[144] P. J. Burnett, T. F. Page, *J. Mater. Sci.* **1985**, *20*, 4624.
[145] H. Jiang, D. Y. Khang, H. Fei, H. Kim, Y. Huang, J. Xiao, J. A. Rogers, *J. Mech. Phys. Solids* **2008**, *56*, 2585.
[146] Z. Huang, W. Hong, Z. Suo, *Phys. Rev. E* **2004**, *70*, 4.
[147] R. Huang, Z. Suo, *J. Appl. Phys.* **2002**, *91*, 1135.
[148] R. Huang, Z. Suo, *Int. J. Solids Struct.* **2002**, *39*, 1791.
[149] R. Huang, H. Yin, J. Liang, J. C. Sturm, K. D. Hobart, Z. Suo, *Acta Mech. Sin. Xuebao* **2002**, *18*, 441.

© 2021 Wiley-VCH GmbH

[150] Z. Y. Huang, W. Hong, Z. Suo, *J. Mech. Phys. Solids* **2005**, *53*, 2101.
[151] R. Huang, *J. Mech. Phys. Solids* **2005**, *53*, 63.
[152] D. Y. Khang, H. Jiang, Y. Huang, J. A. Rogers, *Science* **2006**, *311*, 208.
[153] C. Chen, W. Tao, Z. J. Liu, Y. W. Zhang, J. Song, *Theor. Appl. Mech. Lett.* **2011**, *1*, 021001.
[154] H. Jiang, Y. Sun, J. A. Rogers, Y. Huang, *Int. J. Solids Struct.* **2008**, *45*, 2014.
[155] H. Jiang, Y. Sun, J. A. Rogers, Y. Huang, *Appl. Phys. Lett.* **2007**, *90*, 133119.
[156] K. Nan, H. Luan, Z. Yan, X. Ning, Y. Wang, A. Wang, J. Wang, M. Han, M. Chang, K. Li, Y. Zhang, W. Huang, Y. Xue, Y. Huang, Y. Zhang, J. A. Rogers, *Adv. Funct. Mater.* **2017**, *27*, 1604281.
[157] H. Fu, K. Nan, P. Froeter, W. Huang, Y. Liu, Y. Wang, J. Wang, Z. Yan, H. Luan, X. Guo, Y. Zhang, C. Jiang, L. Li, A. C. Dunn, X. Li, Y. Huang, Y. Zhang, J. A. Rogers, *Small* **2017**, *13*, 1700151.
[158] H. Zhao, K. Li, M. Han, F. Zhu, A. Vázquez-Guardado, P. Guo, Z. Xie, Y. Park, L. Chen, X. Wang, H. Luan, Y. Yang, H. Wang, C. Liang, Y. Xue, R. D. Schaller, D. Chanda, Y. Huang, Y. Zhang, J. A. Rogers, *Proc. Natl. Acad. Sci. U. S. A.* **2019**, *116*, 13239.
[159] H. Fu, K. Nan, W. Bai, W. Huang, K. Bai, L. Lu, C. Zhou, Y. Y. Y. Y. Liu, F. Liu, J. Wang, M. Han, Z. Yan, H. Luan, Y. Y. Y. Y. Zhang, Y. Y. Y. Y. Zhang, J. Zhao, X. Cheng, M. Li, J. W. Lee, Y. Y. Y. Y. Liu, D. Fang, X. Li, Y. Huang, Y. Y. Y. Y. Zhang, J. A. Rogers, *Nat. Mater.* **2018**, *17*, 268.
[160] Y. Zhang, Z. Yan, K. Nan, D. Xiao, Y. Liu, H. Luan, H. Fu, X. Wang, Q. Yang, J. Wang, W. Ren, H. Si, F. Liu, L. Yang, H. Li, J. Wang, X. Guo, H. Luo, L. Wang, Y. Huang, J. A. Rogers, *Proc. Natl. Acad. Sci. U. S. A.* **2015**, *112*, 11757.
[161] Z. Zhao, J. Wu, X. Mu, H. Chen, H. J. Qi, D. Fang, *Sci. Adv.* **2017**, *3*, e1602326.
[162] J.-H. Na, A. A. Evans, J. Bae, M. C. Chiappelli, C. D. Santangelo, R. J. Lang, T. C. Hull, R. C. Hayward, *Adv. Mater.* **2015**, *27*, 79.
[163] D. H. Gracias, *Curr. Opin. Chem. Eng.* **2013**, *2*, 112.
[164] Y. Liu, J. Genzer, M. D. Dickey, *Prog. Polym. Sci.* **2016**, *52*, 79.
[165] C. Dai, J.-H. Cho, *Nano Lett.* **2021**, *21*, 2066.
[166] D. Giambastiani, F. Dispinzeri, F. Colangelo, S. Forti, C. Coletti, A. Tredicucci, A. Pitanti, S. Roddaro, *J. Appl. Phys.* **2020**, *128*, 115104.
[167] R. Li, D. Jin, D. Pan, S. Ji, C. Xin, G. Liu, S. Fan, H. Wu, J. Li, Y. Hu, D. Wu, L. Zhang, J. Chu, *ACS Nano* **2020**, *14*, 5233.
[168] M. Jamal, A. M. Zarafshar, D. H. Gracias, *Nat. Commun.* **2011**, *2*, 527.
[169] Z. Zhao, J. Wu, X. Mu, H. Chen, H. J. Qi, D. Fang, *Macromol. Rapid Commun.* **2017**, *38*, 1600625.
[170] J. K. Park, K. Nan, H. Luan, N. Zheng, S. Zhao, H. Zhang, X. Cheng, H. Wang, K. Li, T. Xie, Y. Huang, Y. Zhang, S. Kim, J. A. Rogers, *Adv. Mater.* **2019**, *31*, 1905715.
[171] A. Besnard, M. R. Ardigo, L. Imhoff, P. Jacquet, *Appl. Surf. Sci.* **2019**, *487*, 356.
[172] J. A. Floro, S. J. Hearne, J. A. Hunter, P. Kotula, E. Chason, S. C. Seel, C. V. Thompson, *J. Appl. Phys.* **2001**, *89*, 4886.
[173] F. Motazedian, Z. Wu, J. Zhang, B. Samsam Shariat, D. Jiang, M. Martyniuk, Y. Liu, H. Yang, *Mater. Des.* **2019**, *181*, 108063.
[174] E. Dobročka, P. Novák, D. Búc, L. Harmatha, J. Murín, *Appl. Surf. Sci.* **2017**, *395*, 16.
[175] J. Todt, H. Hammer, B. Sartory, M. Burghammer, J. Kraft, R. Daniel, J. Keckes, S. Defregger, *J. Appl. Crystallogr.* **2016**, *49*, 182.
[176] I.-T. Bae, T. Ichinose, M.-G. Han, Y. Zhu, S. Yasui, H. Naganuma, *Sci. Reports* **2018**, *8*, 893.
[177] T. Wermelinger, R. Spolenak, *Springer Ser. Opt. Sci.* **2010**, *158*, 259.
[178] X. Wu, J. Yu, T. Ren, L. Liu, *Microelectronics J* **2007**, *38*, 87.
[179] Q. Luo, A. H. Jones, *Surf. Coatings Technol.* **2010**, *205*, 1403.
[180] C. A. Taylor, M. F. Wayne, W. K. S. Chiu, *Thin Solid Films* **2003**, *429*, 190.
[181] T. Peña, S. A. Chowdhury, A. Azizimanesh, A. Sewaket, H. Askari, S. M. Wu, *2D Mater.* **2021**, *8*, 045001.
[182] Q. Li, Y. Gou, T.-G. Wang, T. Gu, Q. Yu, L. Wang, *Coatings* **2019**, *9*, 500.
[183] M. Krottenthaler, C. Schmid, J. Schaufler, K. Durst, M. Göken, *Surf. Coatings Technol.* **2013**, *215*, 247.
[184] W. C. Pan, A. T. Tsai, F. Y. Cheng, T. Y. F. Chen, M. T. Lin, *Conference Proceedings of the Society for Experimental Mechanics*, Springer, New York, **2019**, pp. 109–111.
[185] X. Song, K. B. Yeap, J. Zhu, J. Belnoue, M. Sebastiani, E. Bemporad, K. Y. Zeng, A. M. Korsunsky, *Procedia Engineering*, Elsevier Ltd, Amsterdam, Netherlands **2011**, pp. 2190–2195.
[186] P. J. Withers, H. K. D. H. Bhadeshia, *Mater. Sci. Technol.* **2001**, *17*, 355.
[187] M. Gunda, P. Kumar, M. Katiyar, *Crit. Rev. Solid State Mater. Sci.* **2017**, *42*, 129.
[188] L. B. Freund, S. Suresh, *Thin Film Materials*, Cambridge University Press, Cambridge **2004**.
[189] G. G. Stoney, *Proc. R. Soc. London. A* **1909**, *82*, 172.
[190] X. Y. Feng Huang, A. J. Rosakis, *J. Mech. Mater. Struct* **2005**, *21*, 2220.
[191] N. J. Salamon, C. B. Masters, *Int. J. Solids Struct.* **1995**, *32*, 473.
[192] C. B. Masters, N. J. Salamon, *Int. J. Eng. Sci.* **1993**, *31*, 915.
[193] L. B. Freund, *J. Mech. Phys. Solids* **2000**, *48*, 1159.
[194] T. Wermelinger, R. Spolenak, *Surf. Sci.* **2018**, *66*, 509.
[195] K. Abiko, Y. Kato, H. Hohjo, Y. Kishida, E. Sudo, *J. Raman Spectrosc.* **2020**, *51*, 193.
[196] T. Batten, J. W. Pomeroy, M. J. Uren, T. Martin, M. Kuball, *J. Appl. Phys.* **2009**, *106*, 094509.
[197] A. Qualtieri, F. Rizzi, M. T. Todaro, A. Passaseo, R. Cingolani, M. De Vittorio, *Microelectron. Eng.* **2011**, *88*, 2376.
[198] Q. Zhang, W. Ruan, H. Wang, Y. Zhou, Z. Wang, L. Liu, *Sensors Actuators, A Phys* **2010**, *158*, 273.
[199] A. R. Kermany, F. Iacopi, *J. Appl. Phys.* **2015**, *118*, 155304.
[200] C. Abels, V. Mastronardi, F. Guido, T. Dattoma, A. Qualtieri, W. Megill, M. De Vittorio, F. Rizzi, *Sensors* **2017**, *17*, 1080.
[201] A. Qualtieri, F. Rizzi, G. Epifani, A. Ernits, M. Kruusmaa, M. De Vittorio, *Microelectron. Eng.* **2012**, *98*, 516.
[202] Y. Zhou, Z. Wang, C. Wang, W. Ruan, L. Liu, *J. Micromech. Microeng.* **2009**, *19*, 065026.
[203] G. P. Nikishkov, *J. Appl. Phys.* **2003**, *94*, 5333.
[204] J. M. Zanardi, P. O. Vaccaro, T. Fleischmann, T. S. Wang, K. Kubota, T. Aida, T. Ohnishi, A. Sugimura, R. Izumoto, M. Hosoda, S. Nashima, *Appl. Phys. Lett.* **2003**, *83*, 3647.
[205] O. Jun, P. O. Vaccaro, A. Vorob'ev, T. Tokuda, Y. Sakano, D. Mori, J. Ohta, M. Nunoshita, P. O. Vaccaro, A. Vorob'ev, K. Kubota, N. Saito, *Artic. Electron. Lett.* **2004**, *40*, 1333.
[206] P. O. Vaccaro, K. Kubota, T. Aida, *Appl. Phys. Lett.* **2001**, *78*, 2852.
[207] I. Kao, A. Kumar, J. Binder, *IEEE Sens. J.* **2007**, *7*, 713.
[208] Y. H. Wang, T. H. Hsueh, R. H. Ma, C. Y. Lee, L. M. Fu, P. C. Chou, C. H. Tsai, *2008 Symposium on Design, Test, Integration and Packaging of MEMS/MOEMS*, IEEE, Nice, France **2008**, pp. 142–145.
[209] Y.-H. Wang, C.-Y. Lee, C.-M. Chiang, *Sensors* **2007**, *7*, 2389.
[210] F. Rizzi, A. Qualtieri, L. D. Chambers, G. Epifani, W. M. Megill, M. De Vittorio, *Flow Sensing in Air and Water*, Springer, Berlin Heidelberg, **2014**, pp. 499–519.
[211] C. Giordano, I. Ingrosso, M. Grande, A. Qualtieri, M. Pugliese, M. T. Todaro, V. Tasco, M. De Vittorio, A. Passaseo, *Ferroelectrics*, Taylor & Francis Group, Oxfordshire UK **2009**, pp. 75–82.
[212] W. Zhang, Z. Zhang, Y. Zhang, *Nanoscale Res. Lett.* **2011**, *6*, 555.
[213] Z. Tian, S. Li, S. Kiravittaya, B. Xu, S. Tang, H. Zhen, W. Lu, Y. Mei, *Nano Lett.* **2018**, *18*, 8035.
[214] V. Y. Prinz, V. A. Seleznev, A. K. Gutakovsky, A. V. Chehovskiy, V. V. Preobrazhenskii, M. A. Putyato, T. A. Gavrilova, *Phys. E* **2000**, *6*, 828.

 © 2021 Wiley-VCH GmbH

[215] S. Giudicatti, S. M. Marz, L. Soler, A. Madani, M. R. Jorgensen, S. Sanchez, O. G. Schmidt, *J. Mater. Chem. C* **2014**, *2*, 5892.
[216] S. V. Golod, V. Y. Prinz, V. I. Mashanov, A. K. Gutakovsky, *Semicond. Sci. Technol.* **2001**, *16*, 181.
[217] L. Zhang, S. V. Golod, E. Deckardt, V. Prinz, D. Grützmacher, *Phys. E* **2004**, *23*, 280.
[218] Y. Mei, G. Huang, A. A. Solovev, E. B. Ureña, I. Mönch, F. Ding, T. Reindl, R. K. Y. Fu, P. K. Chu, O. G. Schmidt, *Adv. Mater.* **2008**, *20*, 4085.
[219] Q. Guo, G. Wang, D. Chen, G. Li, G. Huang, M. Zhang, X. Wang, Y. Mei, Z. Di, *Appl. Phys. Lett.* **2017**, *110*, 112104.
[220] F. Cavallo, R. Songmuang, O. G. Schmidt, *Appl. Phys. Lett.* **2008**, *93*, 143113.
[221] F. Cavallo, R. Songmuang, C. Ulrich, O. G. Schmidt, *Appl. Phys. Lett.* **2007**, *90*, 193120.
[222] O. G. Schmidt, K. Eberl, *Nature* **2001**, *410*, 168.
[223] Y. Mei, A. A. Solovev, S. Sanchez, O. G. Schmidt, *Chem. Soc. Rev.* **2011**, *40*, 2109.
[224] S. Moradi, E. S. G. Naz, G. Li, N. Bandari, V. K. Bandari, F. Zhu, H. Wendrock, O. G. Schmidt, *Adv. Mater. Interfaces* **2020**, *7*, 1902048.
[225] I. S. Chun, A. Challa, B. Derickson, K. J. Hsia, X. Li, *Nano Lett.* **2010**, *10*, 3927.
[226] R. Songmuang, C. Deneke, O. G. Schmidt, *Appl. Phys. Lett.* **2006**, *89*, 223109.
[227] I. S. Chun, V. B. Verma, V. C. Elarde, S. W. Kim, J. M. Zuo, J. J. Coleman, X. Li, *J. Cryst. Growth* **2008**, *310*, 2353.
[228] C. Giordano, M. T. Todaro, A. Salhi, L. Martiradonna, I. Viola, A. Passabì, L. Carbone, G. Gigli, A. Passaseo, M. De Vittorio, *Microelectron. Eng.* **2007**, *84*, 1408.
[229] X. Li, *J. Phys. D. Appl. Phys.* **2008**, *41*, 193001.
[230] Z. Tian, W. Huang, B. Xu, X. Li, Y. Mei, *Nano Lett.* **2018**, *18*, 3688.
[231] L. Zhang, E. Ruh, D. Grützmacher, L. Dong, D. J. Bell, B. J. Nelson, C. Schönenberger, *Nano Lett.* **2006**, *6*, 1311.
[232] D. J. Bell, L. Dong, B. J. Nelson, M. Golling, L. Zhang, D. Grützmacher, *Nano Lett.* **2006**, *6*, 725.
[233] Y. Mao, Y. Zheng, C. Li, L. Guo, Y. Pan, R. Zhu, J. Xu, W. Zhang, W. Wu, *Adv. Mater.* **2017**, *29*, 1606482.
[234] L. Xia, W. Wu, J. Xu, Y. Hao, Y. Wang, *Proceedings of IEEE International Conference on Micro Electro Mechanical Systems*, IEEE, Istanbul, Turkey **2006**, pp. 118–121.
[235] W. Huang, S. Koric, X. Yu, K. J. Hsia, X. Li, *Nano Lett.* **2014**, *14*, 6293.
[236] V. Y. Prinz, *Phys. Status Solidi* **2006**, *243*, 3333.
[237] V. Y. Prinz, *Phys. E* **2004**, *24*, 54.
[238] W. M. Choi, J. Song, D. Y. Khang, H. Jiang, Y. Y. Huang, J. A. Rogers, *Nano Lett.* **2007**, *7*, 1655.
[239] H. Jiang, D. Y. Khang, J. Song, Y. Sun, Y. Huang, J. A. Rogers, *Proc. Natl. Acad. Sci. U. S. A.* **2007**, *104*, 15607.
[240] Y. Sun, W. M. Choi, H. Jiang, Y. Y. Huang, J. A. Rogers, *Nat. Nanotechnol.* **2006**, *1*, 201.
[241] D. H. Kim, J. Song, M. C. Won, H. S. Kim, R. H. Kim, Z. Liu, Y. Y. Huang, K. C. Hwang, Y. W. Zhang, J. A. Rogers, *Proc. Natl. Acad. Sci. USA* **2008**, *105*, 18675.
[242] H. C. Ko, M. P. Stoykovich, J. Song, V. Malyarchuk, W. M. Choi, C. J. Yu, J. B. Geddes, J. Xiao, S. Wang, Y. Huang, J. A. Rogers, *Nature* **2008**, *454*, 748.
[243] S. Xu, Y. Zhang, J. Cho, J. Lee, X. Huang, L. Jia, J. A. Fan, Y. Su, J. Su, H. Zhang, H. Cheng, B. Lu, C. Yu, C. Chuang, T. Il Kim, T. Song, K. Shigeta, S. Kang, C. Dagdeviren, I. Petrov, P. V. Braun, Y. Huang, U. Paik, J. A. Rogers, *Nat. Commun.* **2013**, *4*, 1543.
[244] Y. Zhang, H. Fu, Y. Su, S. Xu, H. Cheng, J. A. Fan, K. C. Hwang, J. A. Rogers, Y. Huang, *Acta Mater.* **2013**, *61*, 7816.
[245] N. Salowitz, Z. Guo, Y. H. Li, K. Kim, G. Lanzara, F. K. Chang, *J. Compos. Mater.* **2013**, *47*, 97.
[246] W. L. Sung, C. C. Chen, K. Huang, W. Fang, *J. Micromech. Microeng.* **2015**, *26*, 025003.
[247] K. Huang, P. Peumans, in *Smart Structures and Materials 2006: Sensors and Smart Structures Technologies for Civil, Mechanical, and Aerospace Systems* (Eds: M. Tomizuka, C.-B. Yun, V. Giurgiutiu), SPIE, Bellingham, Washington **2006**, p. 617412.
[248] M. U. Rehman, J. P. Rojas, *Extrem. Mech. Lett.* **2017**, *15*, 44.
[249] J. P. Rojas, A. Arevalo, I. G. Foulds, M. M. Hussain, *Appl. Phys. Lett.* **2014**, *105*, 154101.
[250] K. I. Jang, K. Li, H. U. Chung, S. Xu, H. H. N. Jung, Y. Yang, J. W. Kwak, H. H. N. Jung, J. Song, C. Yang, A. Wang, Z. Liu, J. W. J. Y. Lee, B. J. B. H. B. J. Kim, J. J. H. J. Kim, J. W. J. Y. Lee, Y. Yu, B. J. B. H. B. J. Kim, H. Jang, K. J. Yu, J. J. H. J. Kim, J. W. J. Y. Lee, J. W. Jeong, Y. M. Song, Y. Huang, Y. Zhang, J. A. Rogers, *Nat. Commun.* **2017**, *8*, 15894.
[251] K. Li, X. Cheng, F. Zhu, L. Li, Z. Xie, H. Luan, Z. Wang, Z. Ji, H. Wang, F. Liu, Y. Xue, C. Jiang, X. Feng, L. Li, J. A. Rogers, Y. Huang, Y. Zhang, *Adv. Funct. Mater.* **2019**, *29*, 1806630.
[252] Y. Liu, Z. Yan, Q. Lin, X. Guo, M. Han, K. Nan, K.-C. Hwang, Y. Huang, Y. Zhang, J. A. Rogers, *Adv. Funct. Mater.* **2016**, *26*, 2909.
[253] S. Xu, Z. Yan, K.-I. Jang, W. Huang, H. Fu, J. Kim, Z. Wei, M. Flavin, J. McCracken, R. Wang, A. Badea, Y. Liu, D. Xiao, G. Zhou, J. Lee, H. U. Chung, H. Cheng, W. Ren, A. Banks, X. Li, U. Paik, R. G. Nuzzo, Y. Huang, Y. Zhang, J. A. Rogers, *Science* **2015**, *347*, 154.
[254] S. Xu, Y. Zhang, L. Jia, K. E. Mathewson, K. I. Jang, J. Kim, H. Fu, X. Huang, P. Chava, R. Wang, S. Bhole, L. Wang, Y. J. Na, Y. Guan, M. Flavin, Z. Han, Y. Huang, J. A. Rogers, *Science* **2014**, *344*, 70.
[255] J. Rogers, Y. Huang, O. G. Schmidt, D. H. Gracias, *MRS Bull.* **2016**, *41*, 123.
[256] N. Bassik, G. M. Stern, D. H. Gracias, *Appl. Phys. Lett.* **2009**, *95*, 091901.
[257] P. O. Vaccaro, K. Kubota, T. Fleischmann, S. Saravanan, T. Aida, *Microelectron. J.* **2003**, *34*, 447.
[258] A. A. Tseng, *Small* **2005**, *1*, 924.
[259] X. Tian, Z. Liu, H. Lin, B. Jia, Z. Y. Li, J. Li, *Nanoscale* **2018**, *10*, 16630.
[260] Y. Mao, Y. Pan, W. Zhang, R. Zhu, J. Xu, W. Wu, *Nano Lett.* **2016**, *16*, 7025.
[261] N. S. Rajput, A. Banerjee, H. C. Verma, *Nanotechnology* **2011**, *22*, 485302.
[262] S. Yang, Z. Liu, S. Hu, A. Z. Jin, H. Yang, S. Zhang, J. Li, C. Gu, *Nano Lett.* **2019**, *19*, 3432.
[263] T. Yoshida, A. Baba, T. Asano, *Japanese J. Appl. Phys. 1* **2005**, *44*, 5744.
[264] T. Yoshida, M. Nagao, S. Kanemaru, *Jpn. J. Appl. Phys.* **2010**, *49*, 0565011.
[265] K. Chalapat, N. Chekurov, H. Jiang, J. Li, B. Parviz, G. S. Paraoanu, *Adv. Mater.* **2013**, *25*, 91.
[266] Z. Liu, J. Li, Z. Liu, W. Li, J. Li, C. Gu, Z. Y. Li, *Sci. Rep.* **2017**, *7*, 8010.
[267] Z. Liu, S. Du, A. Cui, Z. Li, Y. Fan, S. Chen, W. Li, J. Li, C. Gu, *Adv. Mater.* **2017**, *29*, 1606298.
[268] A. Cui, Z. Liu, J. J. Li, T. H. Shen, X. Xia, Z. Li, Z. Gong, H. Li, B. Wang, J. J. Li, H. Yang, W. Li, C. Gu, *Light Sci. Appl.* **2015**, *4*, 27817.
[269] Z. Liu, Z. Liu, J. Li, W. Li, J. Li, C. Gu, Z. Y. Li, *Sci. Rep.* **2016**, *6*, 27817.
[270] K. Chalapat, N. Chekurov, J. Li, G. S. Paraoanu, *Nuclear Instruments and Methods in Physics Research Section B: Beam Interactions with Materials and Atoms*, Elsevier, Amsterdam **2012**, pp. 202–205.
[271] M. J. Samayoa, M. A. Haque, P. H. Cohen, *J. Micromech. Microeng.* **2008**, *18*, 095005.
[272] Z. Liu, H. Du, Z. Y. Li, N. X. Fang, J. Li, *APL Photonics* **2018**, *3*, 100803.

© 2021 Wiley-VCH GmbH

[273] Z. Yan, F. Zhang, J. Wang, F. Liu, X. Guo, K. Nan, Q. Lin, M. Gao, D. Xiao, Y. Shi, Y. Qiu, H. Luan, J. H. Kim, Y. Wang, H. Luo, M. Han, Y. Huang, Y. Zhang, J. A. Rogers, *Adv. Funct. Mater.* **2016**, *26*, 2629.
[274] Z. Yan, M. Han, Y. Yang, K. Nan, H. Luan, Y. Luo, Y. Zhang, Y. Huang, J. A. Rogers, *Extrem. Mech. Lett.* **2017**, *11*, 96.
[275] L. H. Dudte, E. Vouga, T. Tachi, L. Mahadevan, *Nat. Mater.* **2016**, *15*, 583.
[276] D. M. Sussman, Y. Cho, T. Castle, X. Gong, E. Jung, S. Yang, R. D. Kamien, *Proc. Natl. Acad. Sci. U. S. A.* **2015**, *112*, 7449.
[277] T. Castle, Y. Cho, X. Gong, E. Jung, D. M. Sussman, S. Yang, R. D. Kamien, *Phys. Rev. Lett.* **2014**, *113*, 245502.
[278] T. Castle, D. M. Sussman, M. Tanis, R. D. Kamien, *Sci. Adv.* **2016**, *2*, 1601258.
[279] Z. Fan, Y. Yang, F. Zhang, Z. Xu, H. Zhao, T. Wang, H. Song, Y. Huang, J. A. Rogers, Y. Zhang, *Adv. Mater.* **2020**, *32*, 1908424.
[280] Z. Yan, M. Han, Y. Shi, A. Badea, Y. Yang, A. Kulkarni, E. Hanson, M. E. Kandel, X. Wen, F. Zhang, Y. Luo, Q. Lin, H. H. H. Zhang, X. X. X. Guo, Y. Y. Huang, K. Nan, S. Jia, A. W. Oraham, M. B. Mevis, J. Lim, X. X. X. Guo, M. Gao, W. Ryu, K. J. Yu, B. G. Nicolau, A. Petronico, S. S. Rubakhin, J. Lou, P. M. Ajayan, K. Thornton, G. Popescu, D. Fang, J. V. Sweedler, P. V. Braun, H. H. H. Zhang, R. G. Nuzzo, Y. Y. Huang, Y. Zhang, J. A. Rogers, *Proc. Natl. Acad. Sci. U. S. A.* **2017**, *114*, E9455.
[281] T. Deng, C. Yoon, Q. Jin, M. Li, Z. Liu, D. H. Gracias, *Appl. Phys. Lett.* **2015**, *106*, 203108.
[282] J. Zanardiocampo, *Microelectron. Eng.* **2004**, *73–74*, 429.
[283] J. S. Randhawa, T. G. Leong, N. Bassik, B. R. Benson, M. T. Jochmans, D. H. Gracias, *J. Am. Chem. Soc.* **2008**, *130*, 17238.
[284] Z. Han, L. Liu, K. Wang, H. Song, D. Chen, Z. Wang, S. Niu, J. Zhang, L. Ren, *J. Bionic Eng.* **2018**, *15*, 409.
[285] C. Abels, A. Qualtieri, T. Lober, A. Mariotti, L. D. Chambers, M. De Vittorio, W. M. Megill, F. Rizzi, *Beilstein J. Nanotechnol.* **2019**, *10*, 32.
[286] H. Liu, S. Zhang, R. Kathiresan, T. Kobayashi, C. Lee, *Appl. Phys. Lett.* **2012**, *100*, 223905.
[287] N. André, B. Rue, G. Scheen, D. Flandre, L. A. Francis, J. P. Raskin, *Sens. Actuators, A* **2014**, *206*, 67.
[288] J. T. Reeder, T. Kang, S. Rains, W. Voit, *Adv. Mater.* **2018**, *30*, 1706733.
[289] M. Sohgawa, D. Hirashima, Y. Moriguchi, T. Uematsu, W. Mito, T. Kanashima, M. Okuyama, H. Noma, *Sens. Actuators, A* **2012**, *186*, 32.
[290] S. M. Won, H. Wang, B. H. Kim, K. Lee, H. Jang, K. Kwon, M. Han, K. E. Crawford, H. Li, Y. Lee, X. Yuan, S. B. Kim, Y. S. Oh, W. J. Jang, J. Y. Lee, S. Han, J. Kim, X. Wang, Z. Xie, Y. Zhang, Y. Huang, J. A. Rogers, *ACS Nano* **2019**, *13*, 10972.
[291] X. Cheng, Z. Liu, T. Jin, F. Zhang, H. Zhang, Y. Zhang, *Nanotechnology* **2021**, *32*, 155506.
[292] A. R. Jalil, H. Chang, V. K. Bandari, P. Robaschik, J. Zhang, P. F. Siles, G. Li, D. Bürger, D. Grimm, X. Liu, G. Salvan, D. R. T. Zahn, F. Zhu, H. Wang, D. Yan, O. G. Schmidt, *Adv. Mater.* **2016**, *28*, 2971.
[293] X. Liu, T. Ma, Y. Xu, L. Sun, L. Zheng, O. G. Schmidt, J. Zhang, *Sens. Actuators B* **2018**, *264*, 92.
[294] L. N. Rodrigues, D. Scolfaro, L. Da Conceição, A. Malachias, O. D. D. Couto, F. Iikawa, C. Deneke, *ACS Appl. Nano Mater.* **2021**, *4*, 3140.
[295] Z. Xu, W. Song, K. B. Crozier, *ACS Photonics* **2018**, *5*, 4993.
[296] Y. Yin, S. Li, S. Böttner, F. Yuan, S. Giudicatti, E. S. G. Naz, L. Ma, O. G. Schmidt, *Phys. Rev. Lett.* **2016**, *116*, 253904.
[297] H. Wang, H. Zhen, S. Li, Y. Jing, G. Huang, Y. Mei, W. Lu, *Sci. Adv.* **2016**, *2*, e1600027.
[298] T. Kipp, H. Welsch, C. Strelow, C. Heyn, D. Heitmann, *Phys. Rev. Lett.* **2006**, *96*, 077403.
[299] C. Strelow, H. Rehberg, C. M. Schultz, H. Welsch, C. Heyn, D. Heitmann, T. Kipp, *Phys. Rev. Lett.* **2008**, *101*, 127403.
[300] J. Wang, D. Karnaushenko, M. Medina-Sánchez, Y. Yin, L. Ma, O. G. Schmidt, *ACS Sens.* **2019**, *4*, 1476.
[301] Y. Yin, J. Wang, X. Lu, Q. Hao, E. S. G. Naz, C. Cheng, L. Ma, O. G. Schmidt, *ACS Nano* **2018**, *12*, 3726.
[302] Z. Liu, Y. Xu, C. Y. Ji, S. Chen, X. Li, X. Zhang, Y. Yao, J. Li, *Adv. Mater.* **2020**, *32*, 1907077.
[303] M. L. Tseng, Z. H. Lin, H. Y. Kuo, T. T. Huang, Y. T. Huang, T. L. Chung, C. H. Chu, J. S. Huang, D. P. Tsai, *Adv. Opt. Mater.* **2019**, *7*, 1900617.
[304] A. A. M. Shimojo, I. C. P. Rodrigues, A. G. M. Perez, E. M. B. Souto, L. P. Gabriel, T. Webster, *Racing for the Surface*, Springer, Berlin **2020**, p. 647.
[305] B. P. Chan, K. W. Leong, *Eur. Spine J.* **2008**, *17*, 467.
[306] S. F. Badylak, T. W. Gilbert, *Semin. Immunol.* **2008**, *20*, 109.
[307] G. Huang, Y. Mei, D. J. Thurmer, E. Coric, O. G. Schmidt, *Lab Chip* **2009**, *9*, 263.
[308] R. Feiner, L. Engel, S. Fleischer, M. Malki, I. Gal, A. Shapira, Y. Shacham-Diamand, T. Dvir, *Nat. Mater.* **2016**, *15*, 679.
[309] X. Wang, R. Feiner, H. Luan, Q. Zhang, S. Zhao, Y. Zhang, M. Han, Y. Li, R. Sun, H. Wang, T. L. Liu, X. Guo, H. Oved, N. Noor, A. Shapira, Y. Zhang, Y. Huang, T. Dvir, J. A. Rogers, *Extrem. Mech. Lett.* **2020**, *35*, 100634.
[310] S. M. Willerth, S. E. Sakiyama-Elbert, *Adv. Drug Delivery Rev.* **2007**, *59*, 325.
[311] D. Antoni, H. Burckel, E. Josset, G. Noel, *Int. J. Mol. Sci.* **2015**, *16*, 5517.
[312] H. Zhao, Y. Kim, H. Wang, X. Ning, C. Xu, J. Suh, M. Han, G. J. Pagan-Diaz, W. Lu, H. Li, W. Bai, O. Aydin, Y. Park, J. Wang, Y. Yao, Y. He, M. T. A. Saif, Y. Huang, R. Bashir, J. A. Rogers, *Proc. Natl. Acad. Sci. U. S. A.* **2021**, *118*, e2100077118.
[313] E. Gultepe, S. Yamanaka, K. E. Laflin, S. Kadam, Y. Shim, A. V. Olaru, B. Limketkai, M. A. Khashab, A. N. Kalloo, D. H. Gracias, F. M. Selaru, *Gastroenterology* **2013**, *144*, 691.
[314] Q. Jin, Y. Yang, J. A. Jackson, C. Yoon, D. H. Gracias, *Nano Lett.* **2020**, *20*, 5383.
[315] K. Malachowski, M. Jamal, Q. Jin, B. Polat, C. J. Morris, D. H. Gracias, *Nano Lett.* **2014**, *14*, 4164.
[316] K. Malachowski, J. Breger, H. R. Kwag, M. O. Wang, J. P. Fisher, F. M. Selaru, D. H. Gracias, *Angew. Chem., Int. Ed.* **2014**, *53*, 8045.
[317] H. W. Huang, F. E. Uslu, P. Katsamba, E. Lauga, M. S. Sakar, B. J. Nelson, *Sci. Adv.* **2019**, *5*, eaau1532.
[318] V. Magdanz, S. Sanchez, O. G. Schmidt, *Adv. Mater.* **2013**, *25*, 6470.
[319] V. Magdanz, S. Sanchez, O. G. Schmidt, *Adv. Mater.* **2013**, *25*, 6581.
[320] C. L. Randall, Y. V. Kalinin, M. Jamal, A. Shah, D. H. Gracias, *Nanomed. Nanotechnol. Biol. Med.* **2011**, *7*, 686.
[321] A. A. Solovev, W. Xi, D. H. Gracias, S. M. Harazim, C. Deneke, S. Sanchez, O. G. Schmidt, *ACS Nano* **2012**, *6*, 1751.
[322] F. Liu, Y. Chen, H. Song, F. Zhang, Z. Fan, Y. Liu, X. Feng, J. A. Rogers, Y. Huang, Y. Zhang, *Small* **2019**, *15*, 1804055.
[323] W. Xu, T. Li, Z. Qin, Q. Huang, H. Gao, K. Kang, J. Park, M. J. Buehler, J. B. Khurgin, D. H. Gracias, *Nano Lett.* **2019**, *19*, 7941.
[324] H.-X. Ji, X.-L. Wu, L.-Z. Fan, C. Krien, I. Fiering, Y.-G. Guo, Y. Mei, O. G. Schmidt, *Adv. Mater.* **2010**, *22*, 4591.
[325] Y. Lee, V. K. Bandari, Z. Li, M. Medina-Sánchez, M. F. Maitz, D. Karnaushenko, M. V. Tsurkan, D. D. Karnaushenko, O. G. Schmidt, *Nat. Commun.* **2021**, *12*, 4967.
[326] J. Deng, H. Ji, C. Yan, J. Zhang, W. Si, S. Baunack, S. Oswald, Y. Mei, O. G. Schmidt, *Angew. Chemie* **2013**, *125*, 2382.
[327] L. Liu, J. Wang, S. Oswald, J. Hu, H. Tang, J. Wang, Y. Yin, Q. Lu, L. Liu, E. Carbó-Argibay, S. Huang, H. Dong, L. Ma, F. Zhu, M. Zhu, O. G. Schmidt, *ACS Nano* **2020**, *14*, 11753.
[328] Z. Xie, R. Avila, Y. Huang, J. A. Rogers, *Adv. Mater.* **2020**, *32*, 1902767.

 © 2021 Wiley-VCH GmbH

[329] H. Fallahi, J. Zhang, H.-P. Phan, N.-T. Nguyen, *Micromachines* **2019**, *10*, 830.
[330] J. G. Grajales-Reyes, B. A. Copits, F. Lie, Y. Yu, R. Avila, S. K. Vogt, Y. Huang, A. R. Banks, J. A. Rogers, R. W. Gereau, J. P. Golden, *Nat. Protoc.* **2021**, *16*, 3072.
[331] J. Ausra, M. Wu, X. Zhang, A. Vázquez-Guardado, P. Skelton, R. Peralta, R. Avila, T. Murickan, C. R. Haney, Y. Huang, J. A. Rogers, Y. Kozorovitskiy, P. Gutruf, *Proc. Natl. Acad. Sci. USA* **2021**, *118*, e2025775118.
[332] J. Choi, S. Chen, Y. Deng, Y. Xue, J. T. Reeder, D. Franklin, Y. S. Oh, J. B. Model, A. J. Aranyosi, S. P. Lee, R. Ghaffari, Y. Huang, J. A. Rogers, *Adv. Healthcare Mater.* **2021**, *10*, 2000722.
[333] A. J. Aranyosi, J. B. Model, M. Z. Zhang, S. P. Lee, A. Leech, W. Li, M. S. Seib, S. Chen, N. Reny, J. Wallace, M. H. Shin, A. J. Bandodkar, J. Choi, A. S. Paller, J. A. Rogers, S. Xu, R. Ghaffari, *J. Invest. Dermatol.* **2021**, *141*, 433.
[334] S. Chandra, J. Li, B. Afsharipour, A. F. Cardona, N. L. Suresh, L. Tian, Y. Deng, Y. Zhong, Z. Xie, H. Shen, Y. Huang, J. A. Rogers, W. Z. Rymer, *IEEE Trans. Biomed. Eng.* **2021**, *68*, 1389.
[335] K. Kwon, H. Wang, J. Lim, K. S. Chun, H. Jang, I. Yoo, D. Wu, A. J. Chen, C. G. Gu, L. Lipschultz, J. U. Kim, J. Kim, H. Jeong, H. Luan, Y. Park, C.-J. Su, Y. Ishida, S. R. Madhvapathy, A. Ikoma, J. W. Kwak, D. S. Yang, A. Banks, S. Xu, Y. Huang, J.-K. Chang, J. A. Rogers, *Proc. Natl. Acad. Sci. U. S. A.* **2021**, *118*, e2020398118.
[336] Y. Yang, M. Wu, A. Vázquez-Guardado, A. J. Wegener, J. G. Grajales-Reyes, Y. Deng, T. Wang, R. Avila, J. A. Moreno, S. Minkowicz, V. Dumrongprechachan, J. Lee, S. Zhang, A. A. Legaria, Y. Ma, S. Mehta, D. Franklin, L. Hartman, W. Bai, M. Han, H. Zhao, W. Lu, Y. Yu, X. Sheng, A. Banks, X. Yu, Z. R. Donaldson, R. W. Gereau, C. H. Good, Z. Xie, Y. Huang, Y. Kozorovitskiy, J. A. Rogers, *Nat. Neurosci.* **2021**, *24*, 1035.
[337] E. Song, Z. Xie, W. Bai, H. Luan, B. Ji, X. Ning, Y. Xia, J. M. Baek, Y. Lee, R. Avila, H.-Y. Chen, J.-H. Kim, S. Madhvapathy, K. Yao, D. Li, J. Zhou, M. Han, S. M. Won, X. Zhang, D. J. Myers, Y. Mei, X. Guo, S. Xu, J.-K. Chang, X. Yu, Y. Huang, J. A. Rogers, *Nat. Biomed. Eng.* **2021**, *5*, 759.

Thanh-An Truong received his Bachelor Degree from Hanoi University of Science and Technology, Vietnam in 2014. He received his Master Degree from National Taiwan University of Science and Technology, Taiwan in 2016. From 2016-2021, he worked as a mechanical engineer in Taiwan. Since 2021, he has been a Ph.D. student at Griffith University. His research interests are flexible and stretchable systems for bio-interfaces, three-dimensional nano/micro-devices, and nano/micro-machining technology.

Nam-Trung Nguyen received his Dipl-Ing, Dr Ing, and Dr Ing Habil degrees from Chemnitz University of Technology, Germany, in 1993, 1997, and 2004, respectively. From 1999 to 2013, he has been an Associate Professor with Nanyang Technological University in Singapore. Since 2013, he has been serving as a Professor and the Director of Queensland Micro- and Nanotechnology Centre of Griffith University, Australia. He is a Fellow of ASME and a Senior Member of IEEE. His research is focused on microfluidics, nanofluidics, micro/nanomachining technologies, micro/nanoscale science, and instrumentation for biomedical applications. One of his current research interests is developing flexible and stretchable systems with bio interface.

Hoang-Phuong Phan received the B.E. and M.E. degrees from The University of Tokyo, Japan in 2011 and 2013, and the Ph.D. degree from Griffith University in 2016. His research interests cover a broad range of semiconductor devices and applications, including integrated sensors, wearable/implantable electronics, 3D bio-electronic interfaces, and surgical robotics. Dr. Phan was a visiting scholar at the XLab, Stanford University, CA, USA in 2017, and at the John Rogers Research Group, Northwestern University, IL, USA in 2019. He serves in the Technical Program Committee of the IEEE MEMS conferences.

© 2021 Wiley-VCH GmbH